junctions between endothelial cells and mural cells (pericytes and vascular smooth muscle cells [VSMCs]).[12] VE-cadherin is required in vivo in the postnatal vasculature to maintain endothelial cell integrity and barrier function.[13,14] Moreover, VE-cadherin associated with VEGF receptor is involved in the regulation of permeability after myocardial ischemia.[15]

In the present study, we investigated the role of VE-cadherin promoter-activated cells in ischemia-induced neovascularization. We demonstrate that VE-cadherin promoter is activated in the pre-existing vascular endothelial cells of bone marrow and heart. In addition, we noticed VE-cadherin promoter is activated in the bone marrow cells and peripheral blood cells presumably corresponding to EPCs/CEPCs and CD45-positive cells preferentially homing to infarcted heart. Thus, we raise the possibility of VE-cadherin–mediated cell–cell contact for effective homing of proangiogenic cells to ischemic tissues.

Materials and Methods

Generation of Transgenic Mice

Cre recombinase driven by VE-cadherin promoter (VE-cad-Cre) mice contained the 4.2-kb VE-cad-Cre transgene (Figure 1A) excised from pBluescript-VE-cad-Cre (online supplement, available at http://circres.ahajournals.org). VE-cad-Cre mice were crossed with LacZ reporter mice (cAct-XstopX-LacZ from the Jackson Laboratory, Bar Harbor, Me) or enhanced green fluorescent protein (GFP) reporter mice (CAG-CAT–enhanced GFP [EGFP] obtained from J. Miyazaki, Osaka University).[16] The offspring were named VE-cadherin promoter-driven LacZ-expressing mice (VE/Z) and VE-cadherin promoter-driven EGFP-expressing mice (VE/EG), respectively. All animal experiments were approved by the animal committee of the National Cardiovascular Center and performed according to the regulation of the National Cardiovascular Center.

Detection of Fluorescence In Vivo

VE/EG embryos and dissected organs from VE/EG mice were examined using an Olympus SZX12 stereo-fluorescent microscope equipped with a VB-6010 charge-coupled device camera. The organs from control mice were imaged next to those from VE/EG mice.

Histochemistry, Immunostaining, Immunofluorescence, and In Situ Hybridization

The procedures of histological examination are described in the online supplement.

Neovascularization Models

To monitor VE-cadherin promoter–activated cells during neovascularization, we used a corneal angiogenesis model of 8-week-old VE/EG mouse and myocardial infarction model. Both methods are described in the online supplement.

Parabiosis Model

Pairs of a 6- to 10-week-old wild-type and VE/Z mice were subjected to parabiotic surgery. Mice were surgically joined from shoulder to femur. One week after parabiotic surgery, the coronary artery was ligated in the wild-type mouse.

Characterization of EGFP-Expressing Cells by Flow Cytometric Analysis

EGFP expression of these cells was analyzed by FACS (fluorescence-activated cell sorting) Calibur (BD Biosciences). EGFP together with cell surface antigen immunostained with phycoerythrin-conjugated anti-CD31 or anti-CD45 were investigated using FACS VantageSE or FACS Aria (BD Biosciences).

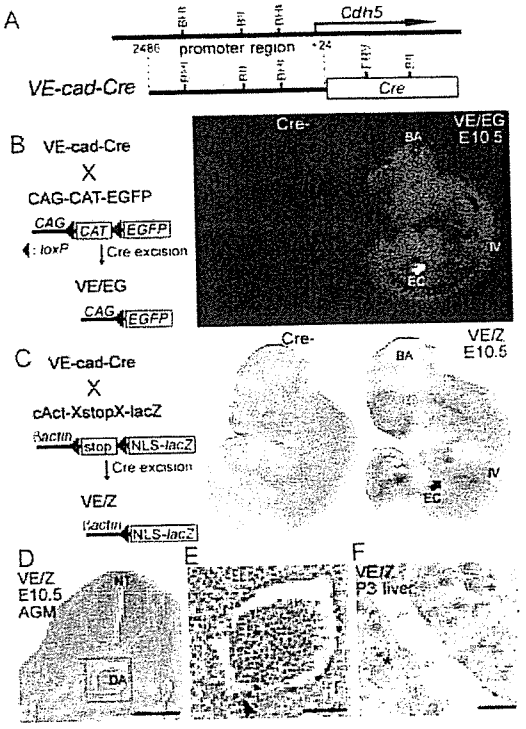

Figure 1. VE-cadherin (Cadherin5, Cdh5) promoter is activated during developmental vascularization. A, VE-cadherin promoter-driven Cre recombinase expressing mouse. BHI, Bam HI; BII, BglII; ERV, EcoRV. B, VE-cadherin promoter-dependent EGFP-expressing mouse (VE/EG). EGFP was expressed in intersomitic vessels (IV), and basilar artery (BA), and endocardium (EC) of VE/EG mice at embryonic day 10.5 (E10.5). No EGFP expression in a littermate lacking *Cre* gene (Cre-). C, VE-cadherin–dependent LacZ-expressing mouse (VE/Z). Whole-mount X-gal staining of E10.5 VE/Z mice shows similar reporter expression to VE/EG. NLS indicates nuclear localization signal. D, Cross-section of neural tube, dorsal aorta, and somites of E10.5 VE/Z embryo shows LacZ-positive signals in dorsal aorta (DA). Bar=200 μm. E, Box in D is enlarged. LacZ-positive cells are present in the hematopoietic cells in the dorsal aorta lumen and its lining cells (arrowhead). Bar=50 μm. F, In the liver, LacZ-expressing cells are detected in the sinusoidal endothelium and the scattered cells, which seem to be hematopoietic cells (asterisks). Bar=20 μm.

Results

VE-Cadherin Promoter Is Activated in Cells Responsible for Developmental Vessel Formation

To trace the VE-cadherin–expressing cells in fetal vascular development and postnatal neovascularization, we first generated transgenic mice expressing VE-cad-Cre (Figure 1A). By crossing three lines of VE-cad-Cre mice with either EGFP reporter mice or LacZ reporter mice, we obtained VE/EG and VE/Z (Figure 1B and 1C).

EGFP and LacZ expression by VE-cad-Cre–mediated recombination was observed in embryonic vascular development (Figure 1B and 1C). We examined LacZ expression in Aorta-Gonad-Mesonephros (AGM) region of VE/Z mice where hemangioblasts reside.[17,18] LacZ-positive cells were detected in the dorsal aorta (Figure 1D, boxed). We noticed that LacZ-stained cells were in the lumen and in the lining cells of the ventral wall (Figure 1E, arrowhead) and in the cells that seemed to bud off from the inner layer. LacZ-

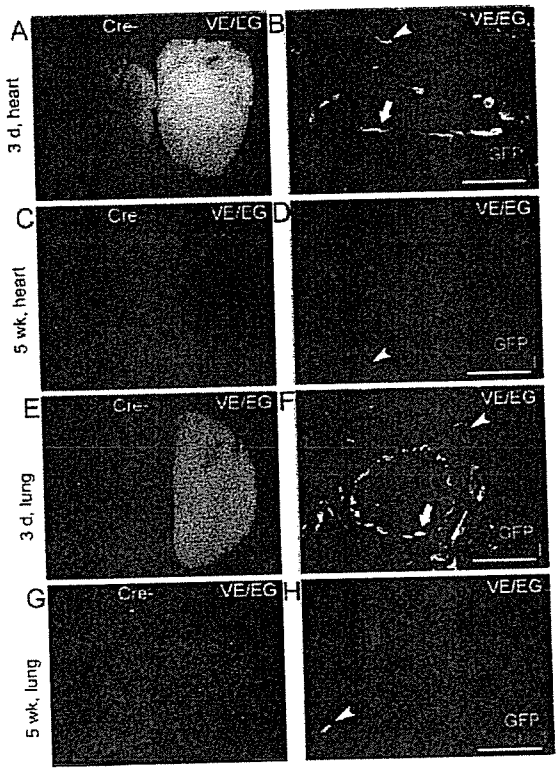

Figure 2. VE-cadherin promoter is less activated after birth than before birth. Organs from littermates lacking *Cre* gene (Cre-) do not show any EGFP expression (A, C, E, and G). A, EGFP is observed in the heart of newborn (3 days after birth) VE/EG mice. B, In the section of a newborn VE/EG mouse heart, EGFP is detected by anti-GFP (green) among the CD31-positive (red) arterial vascular endothelial cells (arrow) and capillary endothelial cells (arrowhead). Positive immunoreaction for anti-GFP and anti-CD31 is visualized by Alexa488-conjugated goat anti-rabbit antibody (green) and Alexa 546-conjugated anti-mouse antibody (red), respectively. C, EGFP is not expressed in the 5-week-old VE/EG mouse heart. D, A few EGFP-positive cells (arrowhead) are detected in capillaries of 5-week-old VE/EG mice. E, Similar to the heart, EGFP is observed in the newborn VE/EG mouse lung. F, EGFP (green) is merged with CD31-positive (red) arterial endothelial cells (arrow) and capillary endothelial cells (arrowhead). G, Lungs of 5-week-old VE/EG mice do not express EGFP. H, A few EGFP-positive cells (arrowhead) were detected in capillaries of the VE/EG mouse lung. Bar=50 μm.

stained cells were also found in the newborn VE/Z mouse liver, where hepatic hematopoiesis is organized (Figure 1F, asterisks). These results suggest that VE-cadherin promoter is activated in the cells probably corresponding to hemangioblasts responsible for fetal vasculogenesis.

VE-Cadherin Promoter Becomes Less Active After Birth

To assess the involvement of VE-cadherin in postnatal vascular development, we examined changes in EGFP reporter expression with age in tissues. Although EGFP expression in both neonatal heart and lung was noticeable, its expression was gradually decreased by aging and no longer observed by the fifth week (Figure 2A, 2C, 2E, and 2G). EGFP and CD31 (platelet and endothelial cell adhesion molecule-1) expression overlapped in the vascular endothelium of both heart and lung of the neonatal VE/EG mice, as revealed by immunohistochemical analyses using anti-GFP

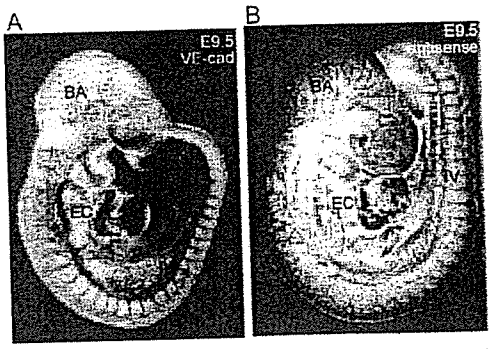

Figure 3. VE-cadherin expression and VE-cadherin mRNA expression in embryogenesis. A, VE-cadherin is detected in the basilar arteries (BA), endocardium (EC), and intersomitic vessels (IV) by immunohistochemistry in an embryonic 9.5 (E9.5) wild-type mouse embryo using anti–VE-cadherin antibody. B, In situ hybridization using antisense probe for VE-cadherin mRNA reveals that VE-cadherin mRNA is expressed in BA, EC, and IV of an E9.5 wild-type mouse embryo. Sense probe used as a negative control does not detect any VE-cadherin mRNA (data not shown). Bar=50 μm.

and anti-CD31 antibodies (Figure 2B and 2F). In clear contrast, GFP was not detected in the CD31-positive vascular endothelium of 5-week-old VE/EG mice (Figure 2D and 2H). Similarly, we found that EGFP expression was decreased with age in other organs, including the brain, liver, and kidney (data not shown).

Tie2 is a tyrosine kinase receptor for angiopoietin and is expressed in the endothelial cells and hematopoietic cells.[19] Thus, we further compared the VE-cadherin promoter-dependent EGFP expression with that dependent on Tie2 promoter. EGFP expression persisted through the entire life (supplemental Figure II), supporting that the VE-cadherin promoter is more active during embryonic and prenatal vascularization than postnatal vessel maintenance. Similarly, VE-cadherin promoter-driven LacZ expression was decreased with aging (supplemental Figure II).

VE-Cadherin Is Expressed in Developing Vasculature

To confirm that VE-cadherin promoter-driven EGFP and LacZ reporter expression reflects endogenous VE-cadherin expression in vivo, we examined the expression of VE-cadherin and VE-cadherin mRNA in embryo. VE-cadherin, VE-cadherin mRNA was detected in developing vessels of the embryo stained with anti–VE-cadherin antibody (Figure 3A) and of the embryo probed with antisense–VE-cadherin cDNA (Figure 3B). VE-cadherin protein and VE-cadherin mRNA were detected in the basilar arteries, intersomitic vessels, and endocardium as reporters of VE/EG and VE/Z mice were expressed. These results indicate that VE-cadherin promoter-driven reporter expression of both VE/EG and VE/Z mice reflects the endogenous VE-cadherin expression.

VE-Cadherin Promoter-Activated Cells Are Involved in Neovascularization

EPCs are positive for VE-cadherin and involved in neovascularization.[6] We hypothesized that VE-cadherin promoter is turned on in EPCs during adult vasculogenesis and that VE-cadherin promoter may be reactivated in vessels. There-

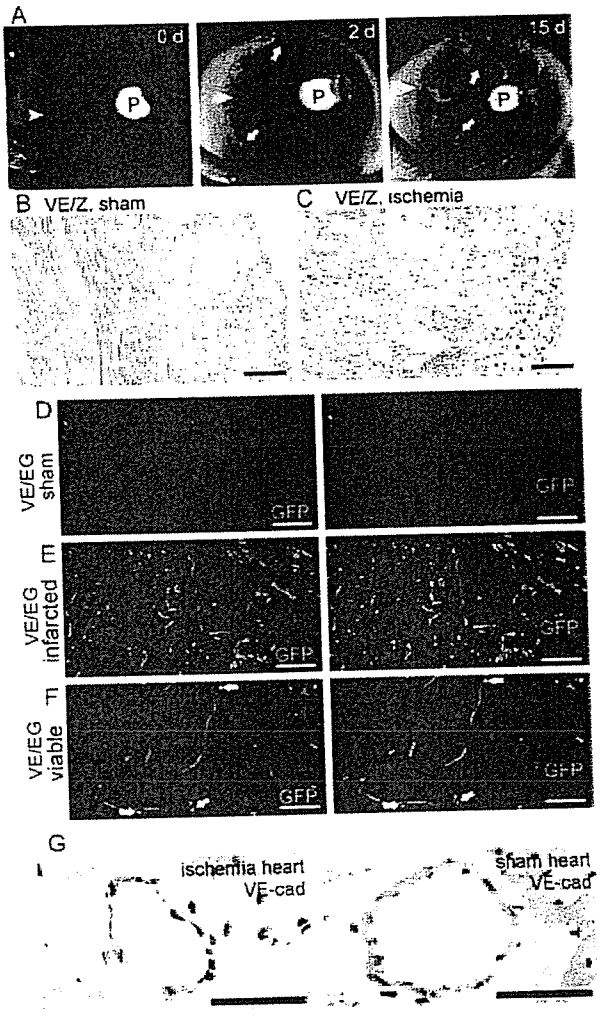

Figure 4. Reactivation of VE-cadherin promoter in response to VEGF and cardiac ischemia. A, New vessel formation monitored by EGFP expression in the VE/EG mouse cornea just 0 days (0 d), 2 days (2 d), and 15 days (15 d) after the implantation of a VEGF-containing pellet (P). Arrowheads and arrows denote the limbus vessels and nascent vessels, respectively. B, Section of sham coronary-ligated VE/Z mouse shows no LacZ-stained cells in the heart. Bar=100 μm C, Numerous LacZ-stained cells are present in the infarcted region of the VE/Z mouse 3 days after coronary ligation. Bar=100 μm. D, The section of the sham-operated VE/EG mouse heart was immunostained with anti-GFP and anti-CD31. Similar to Figure 2, Alexa488 image and that merged with Alexa546 image are shown in the left and right panels, respectively. E, Immunostaining similar to D shows partial colocalization of GFP (green) and CD31 (red) in the infarcted area of VE/EG mouse heart. F, Colocalization of GFP (green) and CD31 (red) in the both arteries and capillaries in the viable area surrounding the infarcted area. Arrowheads denote the GFP-positive cells outside of the endothelium and inside of vascular wall. Bars (in D, E, and F)=50 μm. G, VE-cadherin is detected (brown) in the vessels of infarcted heart but not sham-operated heart. Bar=25 μm.

fore, we first tested whether VEGF induces EGFP expression in using a cornea model of VE/EG mice. After implanting VEGF-containing pellets, EGFP expression was monitored every day. Not only new vessels growing toward the implanted pellets but also limbus vessels exhibited EGFP expression (Figure 4A), indicating that VE-cadherin promoter is activated in the vascular cells involved in neovascularization.

We next tested whether ischemia triggers VE-cadherin expression in a myocardial infarction model. When the coronary artery of VE/Z mice was ligated, LacZ-positive cells were found 3 days after coronary ligation in the hearts of the infarcted mice but not those in the sham-operated mice (Figure 4B and 4C). Similarly, EGFP expression was examined by immunohistochemistry using anti-GFP antibody. In sham-operated control VE/EG mice, GFP-positive cells were not detected in the heart except a few capillaries (Figure 4D), whereas GFP-positive cells were observed in the infarcted area (Figure 4E, left). Notably, among GFP-positive cells, we found CD31-positive cells in the merged image (Figure 4E, right). More than 50% of GFP-positive cells were negative for CD31, suggesting that GFP-positive cells may include nonendothelial lineage cells. Intriguingly, the endothelial cells lining the vessels marked by CD31 in the adjacent viable region were positive for GFP (Figure 4F). In addition, we could find GFP-positive cells in the nonendothelial cell layer in the arterial walls, probably smooth muscle cell layer in the viable area (Figure 4F, arrows). Consistent with GFP reporter expression, VE-cadherin was detected by immunohistochemistry in the endothelium and smooth muscle cells in the vessels of the infarcted heart but not in the sham-operated heart (Figure 4G).

Ischemia Triggers VE-Cadherin Expression in Preexisting Vascular Cells and Mobilized Cells

To test whether the VE-cadherin promoter-activated cells are derived from extracardiac tissues of infarcted mice, we used a parabiotic pairing between a wild-type mouse and a VE/Z mouse (Figure 5, gray mouse and blue mouse, respectively). In a parabiotic mice model, circulating blood cells are mixed through vascular anastomoses that form between the two mice.[20,21] LacZ-positive cells were found in both endothelial cell layer and smooth muscle cell layer of infarcted VE/Z mouse (Figure 5A, arrowhead and arrow, respectively), as confirmed by the same section immunostained with anti-CD31 and anti-α-smooth muscle actin (SMA). In a parabiosis model in which the wild-type mouse was coronary ligated (indicated by cross), we observed that LacZ-positive cells were recruited to the infarcted area of the wild-type mouse (Figure 5B, denoted by cross) from the VE/Z mice (Figure 5B, left). These results indicate that VE-cadherin promoter-reactivated cells are derived from extracardiac tissues and subsequently home to the infarcted heart. Notably, these LacZ-stained cells were negative for CD31 or α-SMA (Figure 5B, right). These results were consistent with those found in the infarcted area of VE/EG mice (Figure 4E). In addition to the infarcted area, LacZ-positive cells were incorporated in the vascular endothelial cell layer and VSMC layer of the viable area (Figure 5C and D), although the number of LacZ-positive cells were much less than that of unconnected mouse. Given that most of the endothelial cells lining the vessels of viable area of infarcted VE/EG mice were positive for GFP (Figure 4E) and that the number of LacZ-positive cells found in the vessels were much less in parabiotic model, VE-cadherin promoter is activated in the pre-existing vessels

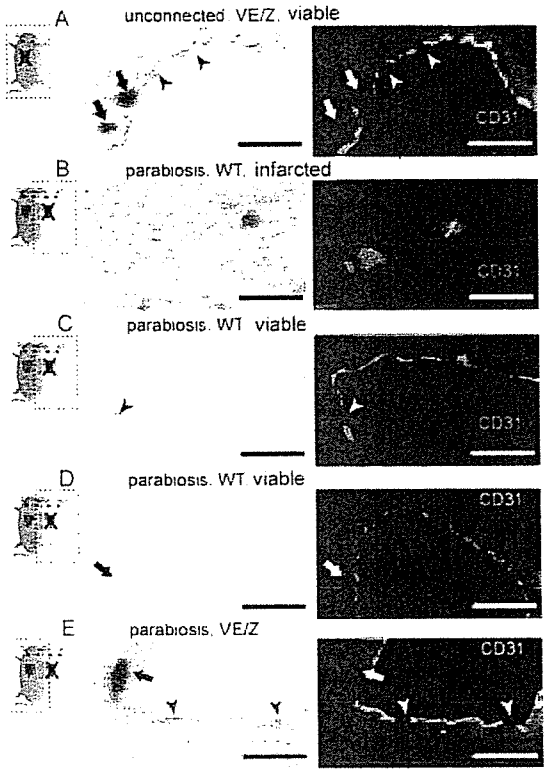

Figure 5. Ischemia induces the recruitment of circulating VE-cadherin promoter-activated cells. Sections show tissues for the mouse indicated by the broken line box. In all panels, crosses indicate coronary ligation, and arrowheads and arrows denote LacZ/CD31-positive and LacZ/α-SMA–positive cells, respectively. All images were obtained by a confocal microscope (LSM510 META; Carl Zeiss). A, LacZ-stained cells in both α-SMA–positive cell layer and CD31-positive cell layer in the arteries of the viable area of infarcted VE/Z mice (cross). B, C, D, and E, A parabiotic pairing between a wild-type (WT) mouse (gray) and a VE/Z mouse (blue). B, Sections of the infarcted heart region of the wild-type mouse were examined for LacZ expression. LacZ-positive cells are negative for CD31 and α-SMA. C and D, In the same model as B, LacZ expression was examined in variable area of infarcted wild-type mouse. E, Coronary arteries of the noninfarcted VE/Z mouse were examined for LacZ expression. Bars=10 μm.

of viable area. Collectively, these data indicate that VE-cadherin–expressing cells, which do not correspond to vascular cells, are recruited to infarcted area from extracardiac tissue. Notably, when examining the heart of the donor VE/Z mouse without myocardial infarction, LacZ-stained cells were found in both endothelial cell layer and VSMC layer in spite of the absence of cardiac ischemia (Figure 5E), indicating that circulating stimuli may activate VE-cadherin promoter in either the pre-existing vascular cells or the mobilized cells from extracardiac tissue to the vasculature. Parabiosis itself did not trigger LacZ expression before the ischemia (supplemental Figure IIIA). Cardiac ischemia, not but other organ ischemia, is critical for VE-cadherin expression in the heart (supplemental Figure III).

VE-Cadherin Promoter Is Activated in Bone Marrow Cells and Circulating Blood Cells on Myocardial Ischemia

To investigate the origin of the cells homing to the ischemic tissues from extracardiac tissue, we explored EGFP-expressing cells in bone marrow and peripheral blood of the infarcted VE/EG mice by flow cytometry. Although EGFP-expressing cells were not detected in the bone marrow of the sham-operated mice, EGFP-expressing bone marrow cells increased after coronary ligation and reached 5% of total bone marrow mononuclear cells (Figure 6A and 6B). In parallel with the increase of EGFP-expressing cells in bone marrow, EGFP-expressing cells also increased in the peripheral blood (Figure 6C). No EGFP-expressing cells were detected in the blood from sham-operated mice. EGFP-expressing cells increased up to 6% of total circulating mononuclear cells 7 days after ligation (Figure 6D).

EGFP-expressing cells were observed in situ in the vasculature as well as in the marrow cells of infarcted VE/EG mice (Figure 6F) but not in sham-operated mice (Figure 6E), suggesting that VE-cadherin–mediated cell adhesion may be involved in mobilization of bone marrow cells into the bloodstream.

We further examined the expression of endogenous VE-cadherin in the EGFP-expressing cells sorted from the bone marrow of infarcted VE/EG mice. More than 90% and 40% of EGFP-expressing cells were positive for VE-cadherin and for CD31, respectively (Figure 6G and 6H). These data indicate that EGFP reporter expression reflects endogenous VE-cadherin expression in bone marrow cells. To characterize the CD31-negative cells, we performed flow cytometric analysis on mononuclear bone marrow cells obtained from infarcted VE/EG mice 2 days after coronary ligation using anti-CD31 and anti-CD45 because CD45 is expressed in the common origin of both myeloid cells and endothelial cells.[5] Among EGFP-positive cells, 50% were positive for CD31, in agreement with the immunostaining of GFP-positive cells with anti-CD31 (Figure 6H and 6I). Of note, all EGFP-expressing cells were positive for the pan-leukocyte cell marker CD45. VE-cadherin mRNAs of bone marrow CD45-positive cells of infarcted mice were twice as much as those of sham-operated mice (supplemental Figure V). These results indicate that EGFP-expressing cells consist of either multilineage cells or distinct stages of differentiated cell from a common origin: CD45-positive EPCs, CD45-positive hematopoietic precursor cells, and CD45-positive hematopoietic cells.

VE-Cadherin Promoter-Activated CD45-Positive Cells Are Actively Recruited to Ischemic Area

We found that VE-cadherin promoter-activated cells were positive for CD45 (Figure 6I) and that CD31-negative GFP-expressing cells were detected in the infarcted area (Figure 4E). Thus, we assumed that CD31-negative GFP-expressing cells might be CD45-positive cells in the infarcted heart. The heart of the infarcted VE/EG mice were immunostained with anti-GFP and anti-CD45. Double-positive staining was found in cells other than elongated cells that seemed to be endothelial cells (Figure 7A). The percentage of double-positive cells among CD45-positive cells in the infarcted area (>10% of CD45-positive cells were positive for GFP) was greater than that of CD45/EGFP-expressing cells in bone marrow cells as examined by FACS analysis (≈1.5% of CD45-positive cells were GFP positive; Figure 6I), indicating that double-positive

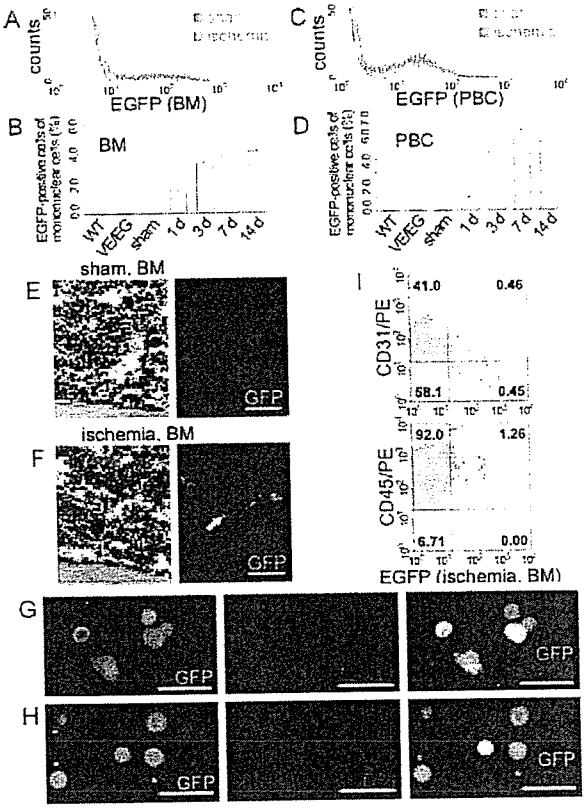

Figure 6. Ischemia induces increases in VE-cadherin promoter-activated bone marrow cells and blood cells. A, Flow cytometric analysis reveals EGFP-expressing cells appearing in bone marrow (BM) 3 days after coronary artery ligation in a VE/EG mouse (green) but not in a sham-operated VE/EG mouse (gray). B, EGFP-expressing cells in bone marrow cells obtained from the infarcted VE/EG mice were counted by flow cytometry. WT indicates wild-type mice; VE/EG, VE/EG mice without any operation; sham, sham-operated VE/EG mice: 1 d, 3 d, 7 d, and 14 d: 1 day, 3 days, 7 days, and 14 days after coronary ligation of VE/EG mice, respectively (n=3). C, Similar to A. EGFP-expressing cells increased in peripheral blood cells (PBC) of the coronary-ligated VE/EG mouse (green) but not in the sham-operated mouse (gray). D, Similar to B. EGFP-expressing peripheral blood cells obtained from infarcted mice were analyzed by flow cytometry. E, Expression of VE-cadherin in BM of sham-operated VE/EG mouse examined by immunostaining with anti-GFP. F, Similar to E. VE-cadherin promoter-reactivated cells were examined in the infarcted VE/EG mouse BM. Arrowheads indicate the immunopositive signal (green) in the endothelium of vessels. Bar=50 μm. G, EGFP-expressing cells obtained by cell sorting from the BM of VE/EG mouse 3 days after coronary ligation were immunostained with anti-GFP (left) and anti-VE-cadherin (center). The GFP image (green) and VE-cadherin image (red) is merged (right). A representative result of more than three independent experiments is shown. H, EGFP-expressing cells obtained from the same mouse as in G were immunostained with anti-GFP (left) and anti-CD31 (center). The merged image is shown in the right panel. I, Bone marrow cells obtained from an infarcted VE/EG mouse 2 days after coronary ligation were immunostained with phycoerythrin (PE)-conjugated anti-CD31 (top) or PE-conjugated anti-CD45 (bottom) and subjected to FACS analysis. Numbers indicate the percentage of cells in the fraction. A representative result of more than three independent experiments is shown.

cells were more selectively recruited to the ischemic area than single CD45-positive cells.

Discussion

Here we show for the first time that VE-cadherin promoter-activated cells are detected in both bone marrow cells and

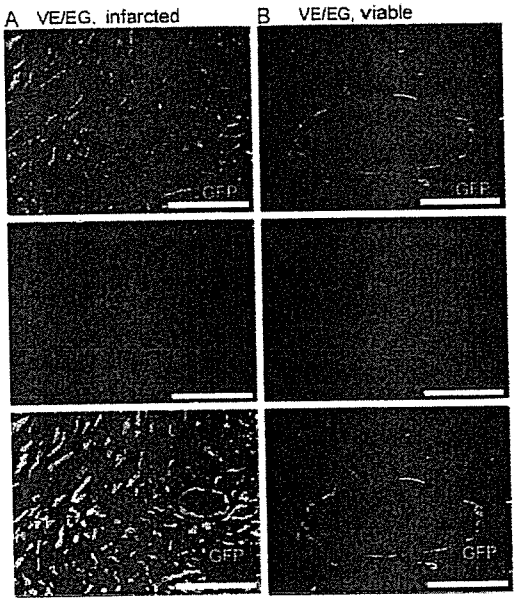

Figure 7. VE-cadherin promoter-activated CD45-positive cells after cardiac ischemia migrate to the infarcted area. A, The infarcted area of the mouse heart immunostained with anti-GFP (top) and anti-CD45 (middle). The GFP image and the CD45 image are merged (bottom). B, The viable area of the same mouse heart was also immunostained with anti-GFP (top), anti-CD45 (middle), and merged (bottom). Bar=100 μm.

blood vessels in the infarcted mice. Although VE-cadherin promoter is less active with aging, reactivated VE-cadherin promoter drives VE-cadherin expression in the pre-existing vessels of ischemic hearts. Our results do not suggest that VE-cadherin is not expressed in mature vessels but rather suggests that VE-cadherin expression is enhanced during ischemia, as detected by anti–VE-cadherin antibody (Figure 4G). Although VE-cadherin is required in the postnatal vascular endothelial cell integrity,[13,14] VE-cadherin is hardly detectable by immunohistochemistry.[22] Ischemia may drive VE-cadherin promoter, resulting in detectable increased VE-cadherin expression in the pre-existing vessels.

What is the role of re-expressed VE-cadherin of the vascular vessels during ischemia? VE-cadherin expression during ischemia may make conditions favorable for the homing of EPCs/CEPCs and the integration of these cells to create the neovessels. VE-cadherin may function not only as an endothelial cell–cell adhesion molecule, but as a leukocyte–endothelial cell adhesion molecule. Leukocytes extravasate across the endothelial cell layer via homophilic platelet and endothelial cell adhesion molecule-1 (CD31), binding between leukocytes and vascular endothelial cells because leukocytes do not express VE-cadherin.[23,24] Because VE-cadherin promoter was activated in CD45-positive leukocytes on ischemia, VE-cadherin on both pre-existing vessels and CD45-positive cells may help to the extravasation of CD45-positive cells.

We noticed that ischemia induced VE-cadherin promoter activation of both marrow cells and endothelium in the bone (Figure 6F). In addition, VE-cadherin promoter-activated marrow cells were positive for VE-cadherin (Figure 6G). VE-cadherin re-expression induced by ischemia appears to pro-

mote the mobilization of VE-cadherin–expressing cells from bone marrow because VE-cadherin regulates the mobilization of bone marrow cells across bone marrow endothelium.[25] Angiopoietin-1/Tie2 signaling maintains an HPC quiescence in bone marrow, probably by regulating N-cadherin.[26] Thus, ischemia may trigger the cadherin switch from N-cadherin to VE-cadherin in cells mobilizing from the bone marrow niche. These CD45-positive cells may function as proangiogenic factor-producing cells at the ischemic tissue.

VE-cadherin may be expressed in both prenatal and postnatal hemangioblasts. In embryos and embryonic stem cells, VE-cadherin–expressing cells have the potential to generate hematopoietic precursors,[27–29] which exist and repopulate in the AGM to differentiate into both hematopoietic cells and endothelial cells.[17] Consistently, we found LacZ-positive cells in the lumen of dorsal aorta and those budding from the lining cells of the dorsal aorta (Figure 1D and 1E). Moreover, no blood cells were found within VE-cadherin–deficient embryos, in addition to impaired vascularization.[30] During embryogenesis, vasculogenesis and hematopoiesis are coordinated by hemangioblasts residing in AGM region, including the dorsal aorta.[31] VE-cadherin–expressing cells may function as adult hemangioblasts because VE-cadherin promoter–activated cells were positive for both CD31 and CD45. It should be tested in the future whether GFP-expressing CD45-positive cells in the infarcted area function as cytokine-secreting cells because EPCs are derived from monocytes and secrete angiogenic factors.[2]

It has been controversial whether bone marrow–derived cells are integrated into vasculature.[32,33] By using parabiotic mice model, we demonstrated that cells from extracardiac tissues were incorporated into both pre-existing endothelial cell and VSMC layers (Figure 5C and 5D). Furthermore, we detected VE-cadherin in both vascular layers of infarcted mice (Figure 4G). VE-cadherin promoter-activated cell detected among smooth muscle cells may be either incorporated cell or pre-existing smooth muscle cells. The former cell may use VE-cadherin–dependent cell–cell interaction for incorporation into the smooth muscle layer across the VE-cadherin–expressing endothelial cells on ischemia. Both endothelial cells and VSMCs originate from the same lineage serving as vascular progenitor cells in embryonic stem cells.[34] Even mature vascular endothelial cells can differentiate into smooth muscle cell.[35] It will be necessary to test whether VE-cadherin promoter-activated cells can give rise to the smooth muscle cells to examine the potential function as vascular progenitor cells.

We obtained the data indicative of unidentified factors that drives VE-cadherin promoter in bone marrow and heart. VEGF-induced mobilization of EPCs depends on the expression of Flk-1 expressed on the EPCs as placental growth factor recruits HPCs that express Flt-1.[8,36] It is of note that we find that circulating factors affect the activity of VE-cadherin promoter just in the vessels of the heart, without affecting activity in other organs (supplemental Figure III). By identifying VE-cadherin promoter-activating factors, we may augment neovascularization in combination with EPC-based cell therapy.

In conclusion, VE-cadherin promoter is reactivated in the ischemic tissue vessels and bone marrow–derived cells. Thus, reactivation of VE-cadherin may be involved in the integration of vessel-constituting cells and angiogenic factor–producing cells.

Acknowledgments

This work was supported by grants from the Ministry of Health, Labor, and Welfare of Japan, from the Program for Promotion of Fundamental Studies in Health Sciences of the National Institute of Biomedical Innovation (NIBIO), from the Ministry of Education, Science, Sports and Culture of Japan, and from Takeda Medical Research Foundation. We thank M. Matsuda for comments; S.I. Nishikawa and D. Vestweber for antibodies; P. Huber for VE-cadherin promoter DNA; M. Yanagisawa, and J. Miyazaki for mice; and M. Miyabayashi, and Y. Matsuura for technical assistance.

References

1. Losordo DW, Dimmeler S. Therapeutic angiogenesis and vasculogenesis for ischemic disease: part II: cell-based therapies. *Circulation*. 2004;109:2692–2697.
2. Rehman J, Li J, Orschell CM, March KL. Peripheral blood "endothelial progenitor cells" are derived from monocyte/macrophages and secrete angiogenic growth factors. *Circulation*. 2003;107:1164–1169.
3. Asahara T, Murohara T, Sullivan A, Silver M, van der ZR, Li T, Witzenbichler B, Schatteman G, Isner JM. Isolation of putative progenitor endothelial cells for angiogenesis. *Science*. 1997;275:964–967.
4. Shi Q, Rafii S, Wu MH, Wijelath ES, Yu C, Ishida A, Fujita Y, Kothari S, Mohle R, Sauvage LR, Moore MA, Storb RF, Hammond WP. Evidence for circulating bone marrow-derived endothelial cells. *Blood*. 1998;92:362–367.
5. Urbich C, Dimmeler S. Endothelial progenitor cells: characterization and role in vascular biology. *Circ Res*. 2004;95:343–353.
6. Rafii S, Lyden D. Therapeutic stem and progenitor cell transplantation for organ vascularization and regeneration. *Nat Med*. 2003;9:702–712.
7. Carmeliet P. Mechanisms of angiogenesis and arteriogenesis. *Nat Med*. 2000;6:389–395.
8. Hattori K, Heissig B, Wu Y, Dias S, Tejada R, Ferris B, Hicklin DJ, Zhu Z, Bohlen P, Witte L, Hendrikx J, Hackett NR, Crystal RG, Moore MA, Werb Z, Lyden D, Rafii S. Placental growth factor reconstitutes hematopoiesis by recruiting VEGFR1(+) stem cells from bone-marrow microenvironment. *Nat Med*. 2002;8:841–849.
9. Takahashi T, Kalka C, Masuda H, Chen D, Silver M, Kearney M, Magner M, Isner JM, Asahara T. Ischemia- and cytokine-induced mobilization of bone marrow-derived endothelial progenitor cells for neovascularization. *Nat Med*. 1999;5:434–438.
10. Carmeliet P. Angiogenesis in health and disease. *Nat Med*. 2003;9:653–660.
11. Dejana E. Endothelial cell-cell junctions: happy together. *Nat Rev Mol Cell Biol*. 2004;5:261–270.
12. Navarro P, Ruco L, Dejana E. Differential localization of VE- and N-cadherins in human endothelial cells: VE-cadherin competes with N-cadherin for junctional localization. *J Cell Biol*. 1998;140:1475–1484.
13. Corada M, Mariotti M, Thurston G, Smith K, Kunkel R, Brockhaus M, Lampugnani MG, Martin-Padura I, Stoppacciaro A, Ruco L, McDonald DM, Ward PA, Dejana E. Vascular endothelial-cadherin is an important determinant of microvascular integrity in vivo. *Proc Natl Acad Sci U S A*. 1999;96:9815–9820.
14. Liao F, Li Y, O'Connor W, Zanetta L, Bassi R, Santiago A, Overholser J, Hooper A, Mignatti P, Dejana E, Hicklin DJ, Bohlen P, Monoclonal antibody to vascular endothelial-cadherin is a potent inhibitor of angiogenesis, tumor growth, and metastasis. *Cancer Res*. 2000;60:6805–6810.
15. Weis S, Shintani S, Weber A, Kirchmair R, Wood M, Cravens A, McSharry H, Iwakura A, Yoon YS, Himes N, Burstein D, Doukas J, Soll R, Losordo D, Cheresh D. Src blockade stabilizes a Flk/cadherin complex, reducing edema and tissue injury following myocardial infarction. *J Clin Invest*. 2004;113:885–894.
16. Kawamoto S, Niwa H, Tashiro F, Sano S, Kondoh G, Takeda J, Tabayashi K, Miyazaki J. A novel reporter mouse strain that expresses enhanced green fluorescent protein upon Cre-mediated recombination. *FEBS Lett*. 2000;470:263–268.

17. de Bruijn MF, Ma X, Robin C, Ottersbach K, Sanchez MJ, Dzierzak E. Hematopoietic stem cells localize to the endothelial cell layer in the midgestation mouse aorta. *Immunity*. 2002;16:673–683.
18. Tavian M, Coulombel L, Luton D, Clemente HS, Dieterlen-Lievre F, Peault B. Aorta-associated CD34+ hematopoietic cells in the early human embryo. *Blood*. 1996;87:67–72.
19. Loughna S, Sato TN. Angiopoietin and Tie signaling pathways in vascular development. *Matrix Biol*. 2001;20:319–325.
20. Wright DE, Wagers AJ, Gulati AP, Johnson FL, Weissman IL. Physiological migration of hematopoietic stem and progenitor cells. *Science*. 2001;294:1933–1936.
21. Abkowitz JL, Robinson AE, Kale S, Long MW, Chen J. Mobilization of hematopoietic stem cells during homeostasis and after cytokine exposure. *Blood*. 2003;102:1249–1253.
22. Ismail JA, Poppa V, Kemper LE, Scatena M, Giachelli CM, Coffin JD, Murry CE. Immunohistologic labeling of murine endothelium. *Cardiovasc Pathol*. 2003;12:82–90.
23. Allport JR, Muller WA, Luscinskas FW. Monocytes induce reversible focal changes in vascular endothelial cadherin complex during transendothelial migration under flow. *J Cell Biol*. 2000;148:203–216.
24. Su WH, Chen HI, Jen CJ. Differential movements of VE-cadherin and PECAM-1 during transmigration of polymorphonuclear leukocytes through human umbilical vein endothelium. *Blood*. 2002;100:3597–3603.
25. van Buul JD, Voermans C, van der Berg V, Anthony EC, Mul FP, van Wetering S, van der Schoot CE, Hordijk PL. Migration of human hematopoietic progenitor cells across bone marrow endothelium is regulated by vascular endothelial cadherin. *J Immunol*. 2002;168:588–596.
26. Arai F, Hirao A, Ohmura M, Sato H, Matsuoka S, Takubo K, Ito K, Koh GY, Suda T. Tie2/angiopoietin-1 signaling regulates hematopoietic stem cell quiescence in the bone marrow niche. *Cell*. 2004;118:149–161.
27. Nishikawa SI, Nishikawa S, Hirashima M, Matsuyoshi N, Kodama H. Progressive lineage analysis by cell sorting and culture identifies FLK1+VE-cadherin+ cells at a diverging point of endothelial and hemopoietic lineages. *Development*. 1998;125:1747–1757.
28. Wang L, Li L, Shojaei F, Levac K, Cerdan C, Menendez P, Martin T, Rouleau A, Bhatia M. Endothelial and hematopoietic cell fate of human embryonic stem cells originates from primitive endothelium with hemangioblastic properties. *Immunity*. 2004;21:31–41.
29. Taoudi S, Morrison AM, Inoue H, Gribi R, Ure J, Medvinsky A. Progressive divergence of definitive haematopoietic stem cells from the endothelial compartment does not depend on contact with the fetal liver. *Development*. 2005;132:4179–4191.
30. Gory-Faure S, Prandini MH, Pointu H, Roullot V, Pignot-Paintrand I, Vernet M, Huber P. Role of vascular endothelial-cadherin in vascular morphogenesis. *Development*. 1999;126:2093–2102.
31. Kubo H, Alitalo K. The bloody fate of endothelial stem cells. *Genes Dev*. 2003;17:322–329.
32. Ziegelhoeffer T, Fernandez B, Kostin S, Heil M, Voswinckel R, Helisch A, Schaper W. Bone marrow-derived cells do not incorporate into the adult growing vasculature. *Circ Res*. 2004;94:230–238.
33. Sata M, Saiura A, Kunisato A, Tojo A, Okada S, Tokuhisa T, Hirai H, Makuuchi M, Hirata Y, Nagai R. Hematopoietic stem cells differentiate into vascular cells that participate in the pathogenesis of atherosclerosis. *Nat Med*. 2002;8:403–409.
34. Yamashita J, Itoh H, Hirashima M, Ogawa M, Nishikawa S, Yurugi T, Naito M, Nakao K, Nishikawa S. Flk1-positive cells derived from embryonic stem cells serve as vascular progenitors. *Nature*. 2000;408:92–96.
35. Frid MG, Kale VA, Stenmark KR. Mature vascular endothelium can give rise to smooth muscle cells via endothelial-mesenchymal transdifferentiation: in vitro analysis. *Circ Res*. 2002;90:1189–1196.
36. Hattori K, Dias S, Heissig B, Hackett NR, Lyden D, Tateno M, Hicklin DJ, Zhu Z, Witte L, Crystal RG, Moore MA, Rafii S. Vascular endothelial growth factor and angiopoietin-1 stimulate postnatal hematopoiesis by recruitment of vasculogenic and hematopoietic stem cells. *J Exp Med*. 2001;193:1005–1014.

Oxidized-HDL_3 modulates the expression of Cox-2 in human endothelial cells

ELISA CALLEGARI[1*], GIUSEPPE D. NORATA[1,3*], HIROYASU INOUE[2] and ALBERICO L. CATAPANO[1,3]

[1]Department of Pharmacological Sciences, University of Milan, Milan, Italy;
[2]Department of Food and Science and Nutrition, Nara Women's University, Nara, Japan;
[3]Center of the Italian Society for the Study of Atherosclerosis, Bassini Hospital, Cinisello Balsamo, Italy

Received January 9, 2006; Accepted March 13, 2006

Abstract. Modified high density lipoprotein (HDL) has been suggested to modulate endothelial expression of pro-inflammatory genes. Since oxidised HDL (Ox-HDL) has been found in atheromatous plaques and receptors for modified HDL are present on endothelial cells, we investigated the effect of Ox-HDL_3 on the expression of Cox-1 or Cox-2. Ox-HDL_3, increased Cox-2 mRNA and protein expression in endothelial cells while no effect on Cox-1 expression was observed. The intracellular pathways involved in this effect were investigated. The incubation with specific inhibitors of intracellular kinases showed that PI3K is mainly involved in the Ox-HDL_3-dependent Cox-2 induction. Transient transfection experiments suggested that the NF-IL6 response element in the proximal promoter (-327 to 59) is involved in Ox-HDL_3-mediated Cox-2 expression. These data suggest that Ox-HDL induce Cox-2 expression in endothelial cells through a PI3K/NF-IL6-dependent pathway.

Introduction

Numerous clinical and epidemiological studies have demonstrated the inverse relationship between HDL cholesterol and the risk of atherosclerosis (1). Beyond the ability of HDL to remove cholesterol from peripheral tissue, HDL particles have additional beneficial effects on the vascular wall (1-3). HDL can inhibit the chemotaxis of monocytes, the adhesion of leukocytes to the endothelium, the LDL oxidation, the endothelial dysfunction and apoptosis. HDL can also act on the vascular tone through the release of vasorelaxant molecule like NO and prostacyclin (PGI2) (3). We have demonstrated previously that HDL increases the release of PGI2 through the induction of cyclooxygenase 2 (Cox-2) and the coupling with PGI syntase in endothelial cells (4). It has been shown that modification of HDL could affect their function (5,6). Oxidised (Ox-) and modified HDL are present in atherosclerotic plaques (7-9) and human analogues of SR-B1 and LOX-1 have been identified as receptors for modified HDL on endothelial cells. *In vitro*, HDL is readily modified using a variety of oxidants (10), with kinetics similar to that reported for LDL (11). Ox-HDL loses its ability to promote cholesterol efflux (5), to induce nitric oxide release (12) and to modulate the expression of matrix-degrading protease and PAI-1 in endothelial cells (13,14).

In the present study, we have investigated the effect of Ox-HDL_3 on the expression of Cox-2 in endothelial cells and the molecular mechanisms involved.

Materials and methods

Materials. HDL subfraction 3 (d 1.125-1.21 g/ml) was obtained from freshly isolated human plasma by preparative ultracentrifugation and dialyzed in PBS containing 0.01% EDTA (15). HDL_3 (1 mg protein/ml) was oxidized with 20 μM Cu_2SO_4 for 24 h at 37˚C, as described (13). The oxidation was blocked by the addition of 40 μM butylated hydroxytoluene (BHT). Under these conditions, we have previously shown that lipoprotein oxidation does not proceed further at 4˚C. The LPS content of HDL_3 was measured using an endotoxin kit from Sigma. No contamination was detected (data not shown). Native HDL_3 and Ox-HDL_3 were used within 6 h of preparation.

The MEK inhibitor, U0126 (New England Biolabs, Germany), the p38 MAPK inhibitor SB 203580 (Sigma, Italy), and the PI3K inhibitor Ly 294002 (Alexis, Italy) were used at a final concentration of 10 μmol/l, 0.5 μmol/l and 50 μmol/l, respectively (15). At these concentrations the inhibitors effectively decreased the phosphorylation of the downstream targets (data not shown).

HUVECs were isolated as described (16) and cultured under standard conditions in medium M-199 containing 20% FCS (fetal calf serum), heparin (15 U/ml) and ECGF (endothelial cell growth factor, 20 μg/ml) (Roche, Italy). The cells

Correspondence to: Dr Giuseppe D. Norata, Department of Pharmacological Sciences, University of Milan, Via Balzaretti 9, I-20133 Milan, Italy
E-mail: danilo.norata@unimi.it

*Contributed equally

Key words: high density lipoprotein, Cox-2, endothelial cells

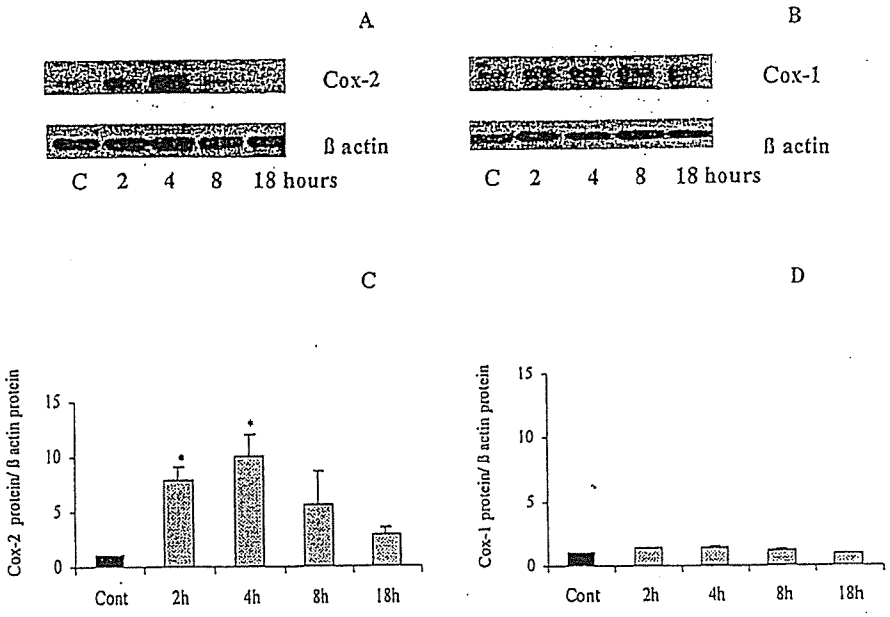

Figure 1. Effect of Ox-HDL$_3$ on Cox-2 and Cox-1 protein expression in endothelial cells. HUVECs were incubated with Ox-HDL$_3$ 30 μg/ml for 2, 4, 8, 18 h. Cells were lysed and the lysates were analysed by immunoblotting using anti Cox-2 (A) and anti Cox-1 (B). The blot was stripped and reprobed with anti ß-actin to confirm equal expression (A and B). Results from 3 different experiments are presented in (C) and (D) (mean ± SD; *p<0.05 vs control cells).

were used within the 4th passage. Cells were plated in 6-well plates and used after 48 h as subconfluent cultures. In all experiments, cells were preincubated with serum-free medium for 6 h, and then native or Ox-HDL$_3$ were added for different times. Cells were incubated in the presence or absence of compounds with appropriate chemicals or vehicle additions (DMSO, 0.1% vol/vol).

Real-time quantitative RT-PCR. Total RNA was extracted and underwent reverse transcription as described (4,17). Three μl of cDNA was amplified by real-time quantitative PCR with 1X SYBER Green universal PCR mastermix (Bio-Rad) (4). The specificity of the SYBER Green fluorescence was tested by plotting fluorescence as a function of temperature to generate a melting curve of the amplicon. The melting peaks of the amplicons were as expected (data not shown). The primers used, the amplicon size and the melting temperature have been described previously (4). Each sample was analyzed in duplicate using the IQ™-Cycler (Bio-Rad). The PCR amplification was related to a standard curve ranging from 10^{-11} M to 10^{-14} M.

Immunoblotting. Cox-1 and Cox-2 expression was investigated as described (18). Briefly, cells were plated in 6-well plates and treated with Ox-HDL$_3$ or native HDL$_3$ for 5-40 min, then lysed using a Tris-glycine buffer (0.25 M Tris, 0.173 M glycine) containing 3% SDS and 1 mM PMSF (phenylmethylsulfonil fluoride). Aliquots of the samples (15 μg) were diluted in a 2% ß-mercaptoethanol buffer containing glycerol and bromophenol blue and electrophoresed on a 12% SDS-PAGE, then transferred onto a nitrocellulose membrane using a Trans Blot Cell (Hoefer Scientific Instrument, San Francisco, CA) (19). The membrane was saturated at room temperature in PBS containing 3% BSA for 1 h, washed with PBS-T (PBS containing 0.1% Tween-20), then incubated overnight at 4°C with a mixture of primary antibody (1:1000 incubation at room temperature for 1 h for Cox-1 and Cox-2 antibodies;

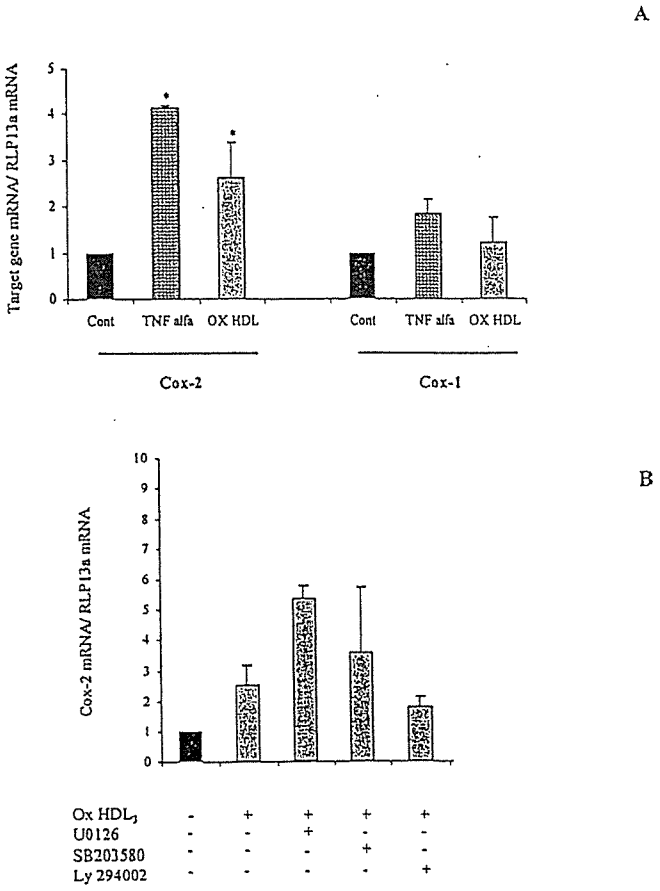

Figure 2. Effects of kinase inhibitors on Ox-HDL$_3$ induced Cox-2 mRNA expression in endothelial cells. (A) HUVECs were incubated for 2 h for mRNA detection with Ox-HDL$_3$ (30 μg/ml), or TNF-α (10 ng/ml) used as positive control. Cox-2 and Cox-1 mRNA expression was measured by quantitative real-time PCR and normalised to RLP13a mRNA expression. (B) HUVECs were incubated for 2 h with Ox-HDL$_3$ (30 μg/ml) alone or in presence of U0126 (10 μM) or SB 203580 (0.5 μM), Ly 294002 (50 μM). Cox-2 mRNA expression was measured by quantitative real-time PCR and normalised to RLP13a mRNA expression. The mean ± SD from 3 different experiments is shown. *p<0.05 vs control cells.

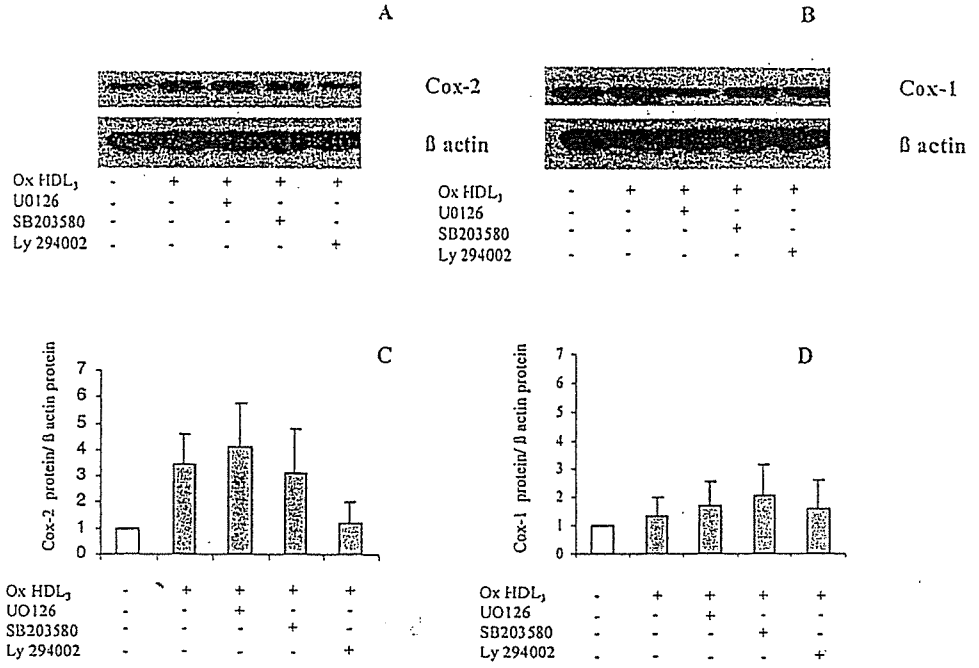

Figure 3. Effects of kinase inhibitors on Ox-HDL_3 induced Cox-2 and Cox-1 protein expression in endothelial cells. HUVECs were incubated for 6 h with Ox-HDL_3 (30 μg/ml) alone or in presence of U0126 (10 μM) or SB 203580 (0.5 μM), Ly 294002 (50 μM) and SH-5 (10 μM). Cells were lysed and the lysates were analysed by immunoblotting using anti Cox-2 (A) and anti Cox-1 (B). The blot was stripped and reprobed with anti ß-actin to confirm equal expression (A and B). Results from 3 different experiments are presented in (C) and (D) (mean ± SD).

1:1000 incubation at room temperature for 1 h for ß-actin antibody) followed by a 1:1000 dilution of peroxidase-conjugated anti-mouse IgG (Sigma) or peroxidase-conjugated anti rabbit IgG (Bio-Rad, Italy). Immunocomplexes were detected by an enhanced chemiluminescence method (ECL, Amersham, Italy), followed by autoradiography and quantified by the Image program (NIH 1.52).

Transfection assay. Transient transfection experiments were first performed using HUVECs and EAhy 926 cells; however, the efficiencies reached were very low with a high degree of cytotoxicity (data not shown). As human Cox-2 promoter regulation is similar in a wide number of cell types we performed transfection experiments in CHO cells, a cell line widely used for studies involving the effects of HDL *in vitro* (4,20). CHO cells were transiently transfected with Cox-2 (nucleotide -327/+59), the NF-κB mutated site (KBM) or the NF-IL6 mutated site (ILM) luciferase reporter vectors using a calcium phosphate precipitation method as described (4). ß-galactosidase activity was assayed as described (14). Luciferase activity was determined and normalized to the ß-gal activity of the cotransfected pSV-ß-galactosidase construct.

Statistical analysis. Data presented in the text and figures are mean ± SD and are representative of 4 different experiments. Statistical analysis was performed by ANOVA with the use of Statsoft Statistica Package.

Results

The experimental set-up was designed to analyse endothelial cell expression of Cox-1 and Cox-2 in the presence of Ox-HDL_3 in relation to basal conditions. The cells were kept in a serum-free medium for 6 h; then HDL_3 (30 μg/ml) or Ox-HDL_3 (30 μg/ml) were added for 4 h. Control cells were incubated for 4 h with the experimental medium containing the same percentage of PBS that was added with the stimulus.

Cox-2 protein was expressed at low levels in unstimulated cells and was strongly induced 2 h after exposure to Ox-HDL_3 (30 μg/ml); the induction was maximal after 4 h and decreased after 8 h (Fig. 1). Cox-2 expression in unstimulated cells remained low at all time points (data not shown). Ox-HDL_3 did not affected Cox-1 protein expression (Fig. 1). Next we examined the effects of Ox-HDL_3 on the Cox-1 and Cox-2 mRNA expression. The cells were kept in a serum-free medium for 6 h; then Ox-HDL_3 (30 μg/ml) or TNF-α (10 ng/ml), used as positive control, were added for 2 h. We observed the induction of Cox-2 mRNA expression by Ox-HDL_3 (30 μg/ml) or TNF-α (10 ng/ml), while no effect was observed on Cox-1 mRNA expression.

To investigate the role of ERK1/2, p38 MAPK and PI3K/Akt pathways in Cox-2 expression induced by Ox-HDL_3, cells were preincubated with the MEK1 inhibitor U0126, the p38 MAPK inhibitor SB 203580 and the PI3K inhibitor Ly 294002 for 1 h; Ox-HDL_3 (30 μg/ml) were then added for 2 and 4 h to evaluate Cox-2 mRNA and protein expression (Figs. 2 and 3). U0126 was unable to block Ox-HDL-induced Cox-2 expression. SB 203580 partially inhibited Ox-HDL-induced Cox-2 expression while Ly 294002 completely abolished Ox-HDL-induced Cox-2 mRNA expression and partially inhibited protein expression. No effect of SB 203580 and Ly 294002 was observed on Cox-1 protein expression.

Next we examined the effects of Ox-HDL on the Cox-2 promoter activity. The human Cox-2 promoter region (-327/+59) contains the NF-κB, the NF-IL6 and the CRE sites

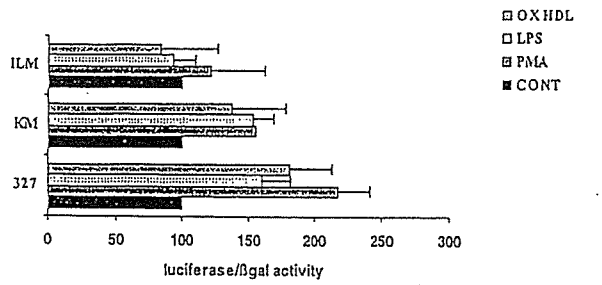

Figure 4. Identification of the regions responsible for Ox-HDL_3-induced promoter activity of the human Cox-2 gene. Following transfection, CHO cells were incubated for 6 h with LPS (1 μg/ml) or PMA (50 ng/ml) both used as positive control, and with Ox-HDL_3 (30 μg/ml). The results are presented as relative luciferase activity normalized to ß-galactosidase activity. Each experiment was carried out in triplicate.

(4,18). Transient transfection assay showed that Ox-HDL induced promoter activity by 199±27% (Fig. 4). PMA, used as positive control, induced promoter activity by 218±35% while LPS induced promoter activity by 160±29% (Fig. 4). Upon incubation with Ox-HDL, the promoter activity of the construct carrying the mutation at the NF-κB site was 140±48%, that of the construct carrying the mutation at the NF-IL6 site was 71±26% (Fig. 4). Upon incubation with PMA the promoter activity of the construct carrying the mutation at the NF-κB site was 155±14%, that of the construct carrying the mutation at the NF-IL6 site was 93±13% (Fig. 4); finally upon incubation with LPS the promoter activity of the construct carrying the mutation at the NF-κB site was 156±24%, that of the construct carrying the mutation at the NF-IL6 site was 83±32% (Fig. 4), thus suggesting a major role of the NF-IL6 site on the effect observed.

Discussion

Several lines of evidence have accumulated indicating that oxidative modification of HDL can occur *in vivo* (10,11,21,22). Furthermore, investigations using the Ox-HDL-specific 9F5-3a antibody have indicated the presence of Ox-HDL in the intima of atheromatous plaques in the human abdominal aorta located specifically in aortic endothelial cells (7), and in sera from patients with chronic renal failure (23). In addition, oxidative modification of HDL not only attenuates its beneficial properties, such as stimulation of cholesterol efflux from foam cells (21), endothelium-dependent vaso-reactivity (24) and anti-oxidative activity (10), but also generates a pro-atherogenic species that inhibits nitric oxide synthesis in endothelial cells (25) and induces production of reactive oxygen species and apoptosis via NF-κB activation (26). Several genes involved in the inflammatory response observed during atherogenesis are modulated through the activation of the NF-κB pathway, including Cox-2 (27).

Here we demonstrated that Ox-HDL could play an harmful role by inducing Cox-2 expression. This effect was specific for Cox-2 as no effect on Cox-1 induction was observed and is dependent upon the activation of intracellular signalling pathways regulating the transcription machinery. We have previously shown that Ox-HDL could modulate PAI-1 expression through the activation of the p38 MAPK pathway promoting RNA stabilization (14). For Ox-HDL-induced Cox-2 expression the p38 MAPK or the ERK1/2 pathway seems to play a minor role, while the activation of the PI3K pathway is fundamental for Ox-HDL-dependent Cox-2 expression in agreement with previous observation with a different experimental setting (28).

To determine the specific transcription factor that is involved in the Ox-HDL mediated Cox-2 expression, we examined the effects of Ox-HDL on the luciferase activity of plasmids containing the Cox-2 promoter defective in the NF-κB or the NF-IL6 binding site (4,18).

Our data clearly demonstrated that the NF-IL6 site is implicated is the response observed. NF-IL6 is a member of the C/EBP family of transcription factors and is involved in inducing several acute-phase protein genes in response to immune and inflammatory stimulation. NF-IL6 also plays a mayor role in inducing the expression of Cox-2 by cytokines and endotoxin (29) thus suggesting that Cox-2 induction by Ox-HDL via NF-IL6 could depend on a pro-inflammatory activated endothelium.

What are the physiological implication(s) of our data? The possibility that Cox-2 plays a harmful role by catalysing the biosynthesis of pro-inflammatory prostanoids has been suggested. Cox-2 immunostaining has been observed in macrophages/foam cells, intimal and medial smooth muscle cells and endothelial cells in atherosclerotic arteries, whereas normal arteries contained no Cox-2 protein (27). Similarly, Schonbeck *et al* (30) found expression of both Cox-1 and Cox-2 by endothelial cells, smooth muscle cells and macrophages in atherosclerotic arteries, while normal arteries only expressed Cox-1. Furthermore, Cox-2 and prostaglandin synthase E colocalize in symptomatic lesions and are possibly involved in metalloprotease activation via PGE_2 production (31) suggesting a role for PGE_2 in plaques instability.

On the other hand, Cox-2 might play an atheroprotective role (27). *In vitro* laminar shear stress upregulates Cox-2 mRNA and protein in HUVEC, turbulent shear stress does not have this effect (32). Prostacyclin is a potent vasodilator, inhibits platelet aggregation and blocks leukocyte adhesion and activation (33). It is therefore possible that Cox-2 induced in endothelial cells at lesion-protected areas catalyses the formation of the anti-atherogenic molecule prostacyclin. These finding suggest the possibility that Cox-2 induction alone is not enough to drive prostaglandin production toward a pro-atherogenic or anti-atherogenic profile, but the prostanoids produced account for this effect. Future studies are thus warranted to identify the prostanoid profile induced by Ox-HDL in the endothelium.

In summary, we have shown that Ox-HDL induces Cox-2 expression in human endothelial cells through a PI3K, NF-IL6-dependent pathway, suggesting a new mechanism by which Ox-HDL could modulate the inflammatory response in the arterial wall.

Acknowledgements

This work was supported by grants from FIRB (2001-RBNE01HLAK_006), COFIN 2004 (2004065985_006 and 2004069574_003), CIRC (Consorzio Interuniversitario Ricerca Cardiovascolare) and SISA Lombardia (Società Italiana Studio Aterosclerosi).

References

1. Norata GD and Catapano AL: Molecular mechanisms responsible for the anti-inflammatory and protective effect of HDL on the endothelium. Vasc Health Risk Manag 1: 119-129, 2005.
2. Nofer JR, Kehrel B, Fobker M, Levkau B, Assmann G and von Eckardstein A: HDL and arteriosclerosis: beyond reverse cholesterol transport. Atherosclerosis 161: 1-16, 2002.
3. Calabresi L, Gomaraschi M and Franceschini G: Endothelial protection by high-density lipoproteins: from bench to bedside. Arterioscler Thromb Vasc Biol 23: 1724-1731, 2003.
4. Norata GD, Callegari E, Inoue H and Catapano AL: HDL3 induces cyclooxygenase-2 expression and prostacyclin release in human endothelial cells via a p38 MAPK/CRE-dependent pathway: effects on COX-2/PGI-synthase coupling. Arterioscler Thromb Vasc Biol 24: 871-877, 2004.
5. Ferretti G, Bacchetti T, Negre-Salvayre A, Salvayre R, Dousset N and Curatola G: Structural modifications of HDL and functional consequences. Atherosclerosis 184: 1-7, 2006.
6. Norata GD, Pirillo A and Catapano AL: Modified HDL: biological and physiopathological consequences. Nutr Metab Cardiovasc Dis 2006.
7. Nakajima T, Origuchi N, Matsunaga T, Kawai S, Hokari S, Nakamura H, Inoue I, Katayama S, Nagata A and Komoda T: Localization of oxidized HDL in atheromatous plaques and oxidized HDL binding sites on human aortic endothelial cells. Ann Clin Biochem 37: 179-186, 2000.
8. Bergt C, Pennathur S, Fu X, Byun J, O'Brien K, McDonald TO, Singh P, Anantharamaiah GM, Chait A, Brunzell J, Geary RL, Oram JF and Heinecke JW: The myeloperoxidase product hypochlorous acid oxidizes HDL in the human artery wall and impairs ABCA1-dependent cholesterol transport. Proc Natl Acad Sci USA 101: 13032-13037, 2004.
9. Zheng L, Nukuna B, Brennan ML, Sun M, Goormastic M, Settle M, Schmitt D, Fu X, Thomson L, Fox PL, Ischiropoulos H, Smith JD, Kinter M and Hazen SL: Apolipoprotein A-I is a selective target for myeloperoxidase-catalyzed oxidation and functional impairment in subjects with cardiovascular disease. J Clin Invest 114: 529-541, 2004.
10. Francis GA: High density lipoprotein oxidation: *in vitro* susceptibility and potential *in vivo* consequences. Biochim Biophys Acta 1483: 217-235, 2000.
11. Thomas MJ, Chen Q, Zabalawi M, Anderson R, Wilson M, Weinberg R, Sorci-Thomas MG and Rudel LL: Is the oxidation of high-density lipoprotein lipids different than the oxidation of low-density lipoprotein lipids? Biochemistry 40: 1719-1724, 2001.
12. Marsche G, Heller R, Fauler G, Kovacevic A, Nuszkowski A, Graier W, Sattler W and Malle E: 2-Chlorohexadecanal derived from hypochlorite-modified high-density lipoprotein-associated plasmalogen is a natural inhibitor of endothelial nitric oxide biosynthesis. Arterioscler Thromb Vasc Biol 24: 2302-2306, 2004.
13. Norata GD, Pellegatta F, Hamsten A, Catapano AL and Eriksson P: Effects of HDL3 on the expression of matrix-degrading proteases in human endothelial cells. Int J Mol Med 12: 73-78, 2003.
14. Norata GD, Banfi C, Pirillo A, Tremoli E, Hamsten A, Catapano AL and Eriksson P: Oxidised-HDL3 induces the expression of PAI-1 in human endothelial cells. Role of p38MAPK activation and mRNA stabilization. Br J Haematol 127: 97-104, 2004.
15. Norata GD, Callegari E, Marchesi M, Chiesa G, Eriksson P and Catapano AL: High-density lipoproteins induce transforming growth factor-beta2 expression in endothelial cells. Circulation 111: 2805-2811, 2005.
16. Norata GD, Pirillo A, Callegari E, Hamsten A, Catapano AL and Eriksson P: Gene expression and intracellular pathways involved in endothelial dysfunction induced by VLDL and oxidised VLDL. Cardiovasc Res 59: 169-180, 2003.
17. Norata GD, Bjork H, Hamsten A, Catapano AL and Eriksson P: High-density lipoprotein subfraction 3 decreases ADAMTS-1 expression induced by lipopolysaccharide and tumor necrosis factor-alpha in human endothelial cells. Matrix Biol 22: 557-560, 2004.
18. Norata GD, Pirillo A, Pellegatta F, Inoue H and Catapano AL: Native LDL and oxidized LDL modulate cyclooxygenase-2 expression in HUVECs through a p38-MAPK, NF-kappaB, CRE dependent pathway and affect PGE2 synthesis. Int J Mol Med 14: 353-359, 2004.
19. Pirillo A, Norata GD, Zanelli T and Catapano AL: Over-expression of inducible heat shock protein 70 in Cos-1 cells fails to protect from cytotoxicity of oxidized ldls. Arterioscler Thromb Vasc Biol 21: 348-354, 2001.
20. Baez JM, Barbour SE and Cohen DE: Phosphatidylcholine transfer protein promotes apolipoprotein A-I-mediated lipid efflux in Chinese hamster ovary cells. J Biol Chem 277: 6198-6206, 2002.
21. Nagano Y, Arai H and Kita T: High density lipoprotein loses its effect to stimulate efflux of cholesterol from foam cells after oxidative modification. Proc Natl Acad Sci USA 88: 6457-6461, 1991.
22. Salmon S, Santus R, Maziere JC, Aubailly M and Haigle J: Modified apolipoprotein pattern after irradiation of human high-density lipoproteins by ultraviolet B. Biochim Biophys Acta 1128: 167-173, 1992.
23. Tsumura M, Kinouchi T, Ono S, Nakajima T and Komoda T: Serum lipid metabolism abnormalities and change in lipoprotein contents in patients with advanced-stage renal disease. Clin Chim Acta 314: 27-37, 2001.
24. Chin JH, Azhar S and Hoffman BB: Inactivation of endothelial derived relaxing factor by oxidized lipoproteins. J Clin Invest 89: 10-18, 1992.
25. Nuszkowski A, Grabner R, Marsche G, Unbehaun A, Malle E and Heller R: Hypochlorite-modified low density lipoprotein inhibits nitric oxide synthesis in endothelial cells via an intracellular dislocalization of endothelial nitric-oxide synthase. J Biol Chem 276: 14212-14221, 2001.
26. Matsunaga T, Hokari S, Koyama I, Harada T and Komoda T: NF-kappa B activation in endothelial cells treated with oxidized high-density lipoprotein. Biochem Biophys Res Commun 303: 313-319, 2003.
27. Linton MF and Fazio S: Cyclooxygenase-2 and inflammation in atherosclerosis. Curr Opin Pharmacol 4: 116-123, 2004.
28. Sheu ML, Chao KF, Sung YJ, Lin WW, Lin-Shiau SY and Liu SH: Activation of phosphoinositide 3-kinase in response to inflammation and nitric oxide leads to the up-regulation of cyclooxygenase-2 expression and subsequent cell proliferation in mesangial cells. Cell Signal 17: 975-984, 2005.
29. Yamamoto K, Arakawa T, Ueda N and Yamamoto S: Transcriptional roles of nuclear factor kappa B and nuclear factor-interleukin-6 in the tumor necrosis factor alpha-dependent induction of cyclooxygenase-2 in MC3T3-E1 cells. J Biol Chem 270: 31315-31320, 1995.
30. Schonbeck U, Sukhova GK, Graber P, Coulter S and Libby P: Augmented expression of cyclooxygenase-2 in human atherosclerotic lesions. Am J Pathol 155: 1281-1291, 1999.
31. Cipollone F, Prontera C, Pini B, Marini M, Fazia M, DeCesare D, Iezzi A, Ucchino S, Boccoli G, Saba V, Chiarelli F, Cuccurullo F and Mezzetti A: Overexpression of functionally coupled cyclooxygenase-2 and prostaglandin E synthase in symptomatic atherosclerotic plaques as a basis of prostaglandin E(2)-dependent plaque instability. Circulation 104: 921-927, 2001.
32. Topper JN, Cai J, Falb D and Gimbrone MA Jr: Identification of vascular endothelial genes differentially responsive to fluid mechanical stimuli: cyclooxygenase-2, manganese superoxide dismutase, and endothelial cell nitric oxide synthase are selectively up-regulated by steady laminar shear stress. Proc Natl Acad Sci USA 93: 10417-10422, 1996.
33. Vane JR and Botting RM: Pharmacodynamic profile of prostacyclin. Am J Cardiol 75: 3A-10A, 1995.

Cox-2 Is Regulated by Toll-Like Receptor-4 (TLR4) Signaling: Role in Proliferation and Apoptosis in the Intestine

MASAYUKI FUKATA,* ANLI CHEN,* ARIELLE KLEPPER,* SUNEETA KRISHNAREDDY,* ARUNAN S. VAMADEVAN,* LISA S. THOMAS,‡ RULIANG XU,§ HIROYASU INOUE,‖ MOSHE ARDITI,¶ ANDREW J. DANNENBERG,# and MARIA T. ABREU*

Inflammatory Bowel Disease Center, Division of Gastroenterology, §Department of Medicine, Department of Pathology Mount Sinai School of Medicine, New York, New York; ¶Division of Pediatric Infectious Diseases, Department of Pediatrics, Steven Spielberg Pediatric Research Center, and ‡Inflammatory Bowel Disease Center, Burns and Allen Research Institute, Cedars-Sinai Medical Center, Los Angeles, California; ‖Department of Food Science and Nutrition, Faculty of Human Life and Environment, Nara Women's University, Nara, Japan; and #Department of Medicine, Division of Gastroenterology and Hepatology, New York Presbyterian Hospital and Weill Medical College of Cornell University, New York, New York

Background & Aims: We recently showed that mice deficient in Toll-like receptor 4 (TLR4) or its adapter molecule MyD88 have increased signs of colitis compared with wild-type (WT) mice after dextran sodium sulfate (DSS)-induced injury. We wished to test the hypothesis that cyclooxygenase 2 (Cox-2)-derived prostaglandin E_2 (PGE_2) is important in TLR4-related mucosal repair. **Methods:** Cox-2 expression was analyzed by real-time polymerase chain reaction, immunohistochemistry, Western blotting, and luciferase reporter constructs. Small interfering RNA was used to inhibit expression of MyD88. TLR4−/− or WT mice were given 2.5% DSS for 7 days. Proliferation and apoptosis were assessed using bromodeoxyuridine staining and terminal deoxynucleotidyl transferase-mediated deoxyuridine triphosphate nick-end labeling assays, respectively. PGE_2 was given orally to DSS-treated mice. **Results:** Intestinal epithelial cell lines up-regulated Cox-2 expression in a TLR4- and MyD88-dependent fashion. Lipopolysaccharide-mediated stimulation of PGE_2 production was blocked by a selective Cox-2 inhibitor or small interfering RNA against MyD88. After DSS injury, Cox-2 expression increased only in WT mice. TLR4−/− mice have significantly reduced proliferation and increased apoptosis after DSS injury compared with WT mice. PGE_2 supplementation of TLR4−/− mice resulted in improvement in clinical signs of colitis and restoration of proliferation and apoptosis to WT values. The mechanism for improved epithelial repair may be through PGE_2-dependent activation of the epidermal growth factor receptor. **Conclusions:** We describe an important link between TLR4 signaling and Cox-2 expression in the gut. TLR4 and MyD88 signaling are required for optimal proliferation and protection against apoptosis in the injured intestine. Although TLR4 signaling is beneficial in the short term, chronic signaling through TLR4 may lower the threshold for colitis-associated cancer.

The intestinal mucosa coexists with a high density of luminal bacteria and pathogen-associated molecular patterns. Indeed, the genetic program of the epithelium is shaped by the presence of bacteria. Compared with germ-free animals, colonization with a single species of gut commensal, *Bacteroides thetaiotaomicron*, results in the expression of genes that enhance barrier fortification and nutrient transport.[1] Early and now more recent studies have shown that germ-free animals have reduced intestinal epithelial cell proliferation compared with colonized mice.[2,3] Finally, germ-free mice are more susceptible to bleeding and death after dextran sodium sulfate (DSS)-induced colitis.[4] These data suggest a link between luminal bacteria and intestinal epithelial repair. Despite the beneficial role of bacteria in the normal function of the intestine, bacteria have been implicated in the pathogenesis of inflammatory bowel diseases (IBDs).[5,6] These disorders are characterized by chronic relapsing intestinal inflammation in the absence of a specific pathogen.

We became interested in the role of Toll-like receptor (TLR) signaling in the intestine as a means to better understand the relationship between epithelial function and bacteria during inflammatory states. TLRs are pattern-recognition receptors expressed by immune and nonimmune cells that signal in response to pathogen-associated molecular patterns expressed by microbes.[7] TLR signaling provides a rapid response against pathogens. Individual or pairs of TLRs recognize distinct pathogen-associated molecular patterns. For example, TLR4 is required for an immune response to lipopolysaccharide (LPS)[8,9] whereas TLR2 in combination with TLR1 recognizes lipoteichoic acid.[10] Most TLR molecules signal through the adapter molecule MyD88 to interleukin-1–receptor–associated kinase and Traf6 to transforming growth factor-β–activated kinase 1, resulting in activation of mitogen activated protein kinases and nuclear translocation of nuclear factor κB.[11]

Several lines of evidence support a role for TLR signaling in intestinal homeostasis. In vitro, TLR ligands induce fortification of intestinal barrier function through redistribution of the tight junction protein Zonula Occludens-1 (ZO-1)[12] and increase expression of β-defensin 2.[13] We and others have used an acute model of colitis to address the function of TLR4 in the setting of epithelial injury and inflammation. Administration of DSS to animals genetically deficient in TLR4 or MyD88 results in greater toxicity manifested by increased rectal bleeding, weight loss, and mortality compared with wild-type (WT) littermates.[14–16] We also have found that animals deficient in

Abbreviations used in this paper: BrdU, bromodeoxyuridine; Cox, cyclooxygenase; DSS, dextran sodium sulfate; EGFR, epidermal growth factor receptor; EIA, enzyme immunoassay; LPS, lipopolysaccharide; PCR, polymerase chain reaction; PGN, peptidoglycan; SD, standard deviation; siRNA, small interfering RNA; TLR, Toll-like receptor; TUNEL, terminal deoxynucleotidyl transferase–mediated deoxyuridine triphosphate nick-end labeling; WT, wild-type; ZO-1, Zonula Occludens-1.

0016-5085/06/$32.00
doi:10.1053/j.gastro.2006.06.017

TLR4 or MyD88 have decreased neutrophil recruitment to the intestine owing to defective expression of chemokines and they experience bacterial translocation to mesenteric lymph nodes.[15] At least part of the reason for the increased bleeding and weight loss may be owing to decreased intestinal epithelial cell proliferation in TLR4 or MyD88 knock-out mice.[3,14,15] This series of observations have led to the conclusion that recognition of luminal bacteria through the intestinal expression of TLRs is important for intestinal homeostasis.

The relationship between epithelial repair and inflammation is complex. An important mediator of both inflammation and repair in the intestine is cyclooxygenase (Cox)-2. Cox-1 and Cox-2 synthesize prostaglandins (PGs) from arachidonic acid.[17] Although intestinal epithelial cells express Cox-1 constitutively, Cox-2 is induced by inflammatory mediators. Cox-2–dependent PGE_2 production is critical for epithelial repair in the intestine in a variety of contexts. In the setting of IBD, increased Cox-2 and PGE_2 have been implicated in the development of colitis-associated cancers.[18,19] We recently showed that microsomal PGE synthase-1, the enzyme that catalyzes the conversion of PGH_2 to PGE_2, is increased in IBD mucosa[18] whereas 15-hydroxyprostaglandin dehydrogenase, the enzyme responsible for catabolism of PGE_2, is reduced in the inflamed mucosa of IBD.[19] This combination results in overall increases in mucosal PGE_2, and the potential for enhanced carcinogenesis in the setting of inflammation.

We wished to better understand the cellular and molecular mechanisms by which TLR4 signaling is involved in intestinal homeostasis. Studies performed before the identification of TLR4 found that systemic administration of LPS protected animals from radiation-induced injury in the gut characterized by apoptosis of intestinal stem cells.[20,21] The mechanism for the LPS-induced radioprotection was found to be induction of Cox-2 and PGE_2 production.[21] In addition, DSS administration to Cox-2 knock-out mice results in a phenotype reminiscent of that seen in TLR4−/− mice, namely increased bleeding and increased mortality.[22]

In the current study, we test the hypothesis that Cox-2–derived PGE_2 is important in TLR4-dependent mucosal homeostasis. Our data show that TLR4-deficient mice fail to up-regulate Cox-2 expression in response to epithelial injury. Both intestinal epithelial cells and lamina propria macrophages express Cox-2 in a TLR4- and MyD88-dependent fashion. PGE_2 is decreased in the mucosa of TLR4−/− mice after DSS injury. Oral supplementation with PGE_2 results in increased intestinal epithelial cell proliferation and decreased apoptosis in DSS-treated TLR4−/− mice. At least part of the mechanism for TLR4-dependent mucosal healing involves activation of epidermal growth factor receptor (EGFR) signaling. The results of our studies shed an important light on the previously unrecognized role of TLR signaling in the regulation of Cox-2 in the gut.

Materials and Methods

Mice and Interventions

TLR4−/− mice and MyD88−/− mice were purchased from Oriental Bio Service, Inc. (Kyoto, Japan). All knock-out mice used were back-crossed to C57Bl/6 mice more than 8 times. C57Bl/6 mice were obtained from Jackson Laboratory as controls (Bar Harbor, ME). Seven- to 10-week-old sex-matched mice were given 2.5% DSS (molecular weight, 36–50 kilodaltons; ICN, Aurora, OH) in their drinking water and were killed at the end of 7 days of DSS treatment. For recovery studies, DSS was administered for the first 7 days as indicated, and then DSS was removed from the drinking water and mice were killed 7 days after the cessation of DSS treatment. PGE_2 (Cayman, Ann Arbor, MI) was diluted from the ethanol stock (10 $\mu g/\mu L$) in phosphate-buffered saline (PBS) and 200 μg in 150 μL was given twice daily by gavage feeding, starting 3 hours before first DSS administration as described previously.[23,24] Control mice were given PBS including the same dilution of ethanol. All experiments were performed according to the Mount Sinai School of Medicine Animal Experimental Ethics Committee guidelines.

Assessment of Colitis Activity

Body weight was assessed at baseline and every day for the duration of the experiment. Weight change was calculated as the percentage change in weight compared with baseline. Fecal blood was tested daily using Hemoccult cards (Beckman Coulter, Inc., Fullerton, CA) and graded as follows: 0 = no blood, 1 = trace blood, 2 = positive, and 4 = gross blood. Mice were euthanized by CO_2 followed by cervical dislocation. The cecum was removed and the remainder of the colon was divided into proximal and distal halves. Tissue was fixed in 10% buffered formalin, paraffin-embedded, sectioned, and stained with H&E. Histologic assessment was performed by a pathologist blinded to the mouse genotype and treatment. Histologic score was a combined score of acute inflammatory cell infiltrate (0–4), chronic inflammatory cell infiltrate (0–3), and crypt damage (0–4).[25–27] Specifically, the crypt damage was scored in the following manner. A score of 0 was given to an intact crypt, 1 = loss of the basal one third of the crypt; 2 = loss of the basal two thirds of the crypt; 3 = entire loss of crypt; and 4 = loss of crypt and surface epithelium.[26] Because the injury from DSS is patchy, 2 slides from each section of the colon were assessed per mouse and at least 3 areas on each slide were examined.

Cell Lines and Reagents

Human intestinal cell lines SW480 and T84 (1×10^6 cells/well) and mouse macrophage cell line RAW264.7 (1.5×10^6 cells/well) (American Type Culture Collection, Manassas, VA) were maintained in Dulbecco's modified Eagle medium supplemented with 10% heat-inactivated fetal calf serum, 2 mmol/L L-glutamine, 5% penicillin/streptomycin, and were incubated in 6-well plates overnight at 37°C in a 5% CO_2 humidified incubator. Cells were incubated with phenol-water–extracted *Escherichia coli* K235 LPS (Sigma, St. Louis, MO), synthetic bacterial lipoprotein (Pam3CSK4) (InvivoGen, San Diego, CA), peptidoglycan (PGN) (InvivoGen), or vehicle for the indicated periods of time. Cox inhibitor NS398 and indomethacin (Sigma) were added at the same time as LPS. AG1478, an EGFR tyrosine kinase inhibitor, was added 30 minutes before LPS stimulation. Recombinant human EGF (R&D Systems, Minneapolis, MN) was used as a control.

Real-Time Polymerase Chain Reaction

Total RNA was isolated by using RNA Bee (Tel-Test, Inc., Friendwood, TX) according to the manufacturer's instructions. A total of 1 μg RNA was used as the template for single-strand complementary DNA (cDNA) synthesis using the Transcriptor First Strand cDNA Synthesis Kit (Roche, India-

Table 1. Sequence of the Primers and Probes Used

Gene	Forward primer	Reverse primer	Probe
Human			
Cox-2	GCA CGT CCA GGA ACT CCT CA	GGG GTA GGC TTT GCT GTC TG	CCT TCA GCT CCA CAG CCA GAC GCC
MyD88	CTC CTC CAC ATC CTC CCT TCC	CCG CAC GTT CAA GAA CAG AGA	CGC CGC ACT CGC ATG TTG AGA GCA
β-actin	GAC TGA GTC TTG CTC TGT CGG	GGC ATG ATG GCT TAC GCC TAT A	AGC GAC TCC TGT GCC TCA GCC TCC
Mouse			
Cox-1	AAG GAG TCT CTC GCT CTG GTT T	TCT CAG GGA TGG TAC AGT TGG G	TGC TCC TGC TGC TGC CGC CGA
Cox-2	ATC CTG CCA GCT CCA CCG	TGG TCA AAT CCT GTG CTC ATA CAT	ACT GCC ACC TCC GCT GCC ACC T
β-actin	ATG ACC CAG ATC ATG TTT GA	TAC GAC CAG AGG CAT ACA	CGT AGC CAT CCA GGC TGT GC

NOTE. Sequences are listed in 5′ to 3′ direction.

napolis, IN) according to the manufacturer's instructions. Quantitative real-time polymerase chain reaction (PCR) was performed for Cox-2, MyD88, Cox-1, and β-actin using TaqMan (Applied Biosystems, Foster City, CA) probes (Table 1). All TaqMan probes and primers were designed using Beacon Designer 3.0 (Premier Biosoft International, Palo Alto, CA) (Table 1). The cDNA was amplified using TaqMan universal PCR Master Mix (Roche) on the ABI Prism 7900HT sequence detection system (Applied Biosystems), programmed for 95°C for 10 minutes, then 40 cycles of 95°C for 15 seconds, and 60°C for 1 minute. The amplification results were analyzed using SDS 2.2.1 software (Applied Biosystems) and the genes of interest were normalized to the corresponding β-actin results. Data were expressed as fold induction relative to the lowest one.

RNA Interference

SW480 cells were plated at a density of 1.5×10^5 cells/well in 12-well plates 24 hours before the first transfection. MyD88 small interfering RNA (siRNA) oligonucleotide corresponding to the sequence (GCUCAUCGAAAAGAGGUGCtt) was purchased from Ambion (Austin, TX) and 50 nmol/L of siRNA were transfected twice every 24 hours with X-trim gene siRNA transfection reagent (Roche) as per the manufacturer's instructions. Forty-eight hours after the first transfection, cells were stimulated with LPS for the indicated period of time. siRNA (50 nmol/L), which has no significant homology to any known gene sequences from mouse, rat, or human being, and siRNA against glycerol dehyde-3-phosphate dehydrogenase were used as negative controls (Ambion).

Western Blot Analysis

Whole-cell lysates were prepared from colonic tissue samples or SW480 cells after treatment with different stimuli using a lysis buffer containing 50 mmol/L Tris HCl, 50 mmol/L NaF, 1% Triton X-100, 2 mmol/L ethylenediaminetetraacetic acid [EDTA], and 100 mmol/L NaCl, with a proteinase inhibitor cocktail (Calbiochem, San Diego, CA). The protein concentration was determined by the Bradford method using Bio-Rad Protein Assay Dye and SmartSpec 3000 (Bio-Rad Laboratories, Hercules, CA). A total of 25 μg of the lysates were subjected to 8% or 10% sodium dodecyl sulfate-polyacrylamide gel electrophoresis and transferred to Immobilon-P membranes (Millipore Corporation, Bedford, MA). The membrane was blocked in 5% skim milk and was immunoblotted with the primary antibodies for 1 hour, followed by horseradish-peroxidase-conjugated secondary antibodies rabbit anti-mouse or goat anti-rabbit IgG (Zymed Laboratories, South San Francisco, CA). The membrane was exposed on radiographic film using an enhanced chemiluminescent substrate SuperSignal West Pico Trial Kit (Pierce Biotechnology, Rockford, IL). Antibodies specific for murine or human Cox-2 were purchased from Cayman. Anti-MyD88 antibody (HFL-296) was purchased from Santa Cruz Biotechnology (Santa Cruz, CA).

Immunofluorescent and Immunohistochemical Studies

Cecum, proximal, and distal colon were freshly isolated and frozen in Optimal Cutting Temperature (OCT; Sakura Finetek, Torrance, CA) or fixed in 10% neutral buffered formalin and embedded in paraffin wax. Part of the samples were fixed with modified Bouin's fixative consisting of 0.5% paraformaldehyde acetate and 15% (vol/vol) of saturated picric acid in 0.1 mol/L PBS pH 7.0. Frozen sections prefixed by modified Bouin's fixation were incubated in 10% normal goat serum for 1 hour and stained with antimurine Cox-2 antibody (1:200; Cayman) overnight at 4°C, followed by TRITC (tetramethyl rhodamine isothiocyanate)-conjugated anti-rabbit IgG (1:200, Zymed Laboratories) for 1 hour at room temperature. The specificity of staining was confirmed using Cox-2 blocking peptide (Cayman) according to the manufacturer's instructions or using rabbit isotype control antibody instead of the primary antibody (Zymed Laboratories).

Double-immunofluorescent staining of CD68 and Cox-2 was performed using prefixed OCT sections. Sections were incubated with 0.1% trypsin (Sigma) $CaCl_2$ dissolved in 0.05 mol/L Tris-Hcl pH 7.6 for 15 minutes at 37°C. Subsequently sections were blocked in 5% skim milk for 1 hour and then incubated with the rat anti-CD68 antibody (1:20, MCA1957S; Serotec Ltd., Raleigh, NC) overnight at 4°C. After washing in PBS, sections were incubated with TRITC-conjugated rabbit anti-rat IgG (1:200; Sigma) for 1 hour at room temperature. Then sections were re-incubated with 5% skim milk followed by Cox-2 staining as described previously using fluorescein isothiocyanate-conjugated goat anti-rabbit IgG (1:200, Sigma).

Phospho-specific EGFR staining was performed using OCT sections. After blocking with 5% milk, sections were incubated with anti-phospho-EGFR antibody (1:200; Santa Cruz) overnight at 4°C. Secondary antibody (fluorescein isothiocyanate-conjugated anti-goat IgG; Sigma) was used at a dilution of 1:200. As a negative control, primary antibody was omitted and tissue was stained with secondary antibody alone. To quantify the expression level of phospho EGFR, staining intensity was analyzed using MetaMorph software (Universal Imaging Corporation, Downingtown, PA). Epithelial cells were selected randomly and the average pixel intensities from 10 areas of gated cells per slide were analyzed to compare the expression levels of phospho EGFR.

Staining of SW480 was performed using 4-chamber slides (Nalgene Nunc International, Rochester, NY), in which cells were

seeded at a density of 1×10^5 cells/well on the day before the experiment. Cells were stained with goat anti-EGFR or anti-phospho-EGFR antibodies (dilution of 1:300) after methanol fixation and preparation with 0.5% Triton X-100. Nonspecific binding was blocked with 5% skim milk. Fluorescein isothiocyanate-conjugated goat anti-rabbit or sheep anti-mouse IgG (1:200; Sigma) was used as a secondary antibody.

SW480 and double-stained tissue slides were examined using a Leica TCS-SP (UV) confocal microscope (Leica, Bannockburn, IL). Four thin optical sections through the x-y axis were acquired. Other slides were viewed on a Nikon eclipse E600 immunofluorescence microscope (Nikon, Melville, NY) and photographs were taken with a digital camera using Spot Advanced software program (Diagnostic Instruments Inc., Sterling Heights, MI).

Assessment of Proliferation and Apoptosis

The number of proliferating cells was detected by immunoperoxidase staining for the thymidine analog bromodeoxyuridine (BrdU). At 1.5 hours before death, mice were injected intraperitoneally with 5-bromo-2'-deoxyuridine (Sigma) at a concentration of 100 mg/kg. Sections (4 μm) of paraffin-embedded colonic tissue were deparaffinized and incubated with 3% H_2O_2 in methanol for 15 minutes. Sections were incubated with 2 N HCl for 1 hour, washed in PBS, and then incubated in 0.1% trypsin for 15 minutes at 37°C. Sections were stained for BrdU incorporation using a BrdU staining kit (Zymed Laboratories Inc.) according to the manufacturer's instructions. The number of BrdU-positive cells per well-oriented crypt was calculated in every 3 crypts for each colon segment at high magnification under light microscopy.

Apoptotic cells in the colonic epithelial cells were detected using the terminal deoxynucleotidyl transferase–mediated deoxyuridine triphosphate nick-end labeling (TUNEL) assay (ApopTaq *In Situ* Apoptosis Detection Kit; Chemicon, Temecula, CA), following the manufacturer's instruction. Briefly, paraffin sections were prepared with proteinase K (20 μg/mL). After equilibration with terminal deoxynucleotidyl transferase buffer, sections were reacted with terminal deoxynucleotidyl transferase enzyme for 1 hour at 37°C. Digoxigenin-labeled free 3'-OH end of DNA was detected by anti-digoxigenin-rhodamine conjugate. Sections were counterstained with 4',6-diamidino-2-phenylindole. The apoptotic cells were counted as follows: 300 epithelial cells were counted per high-power field and scored for apoptosis; a total of 3 fields were counted per section of mouse colon (ie, cecum, proximal, and distal colon). Three mouse colons were counted per condition. The apoptotic index was determined by the ratio of TUNEL-positive nuclei to 100 total nuclei in the epithelial cells counted. The areas of necrosis such as in an ulcer bed were identified by examining the corresponding H&E slides and were excluded from counting for apoptotic cells as previously described.[28]

Transient Gene Expression and Reporter Gene Assays

SW480 cells were plated in 12-well plates at a density of 1.5×10^5 cells/well. Cells were transfected the following day with FuGENE 6 transfection reagent (Roche) as per the manufacturer's instructions. Reporter genes for pRL-TK (0.05 μg), Cox-2 promoter-luciferase constructs (phPES2 −1432/+59: 0.3 μg),[29,30] which were provided by Dr Inoue (Nara Women's University, Nara city, Japan), pGL3 basic empty vector (0.3 μg) were cotransfected as indicated in Figure 1. After overnight transfection, cells were stimulated with LPS (5 μg/mL) for 4 hours. Cells then were lysed and firefly luciferase activity was measured with a Dual-Luciferase Reporter Assay (Promega, San Luis Obispo, CA). Luciferase measurements were normalized to the relative light units from Renilla luciferase from pRL-KT. For experiments in which the Cox-2 promoter and siRNA against MyD88 were used, the siRNA (50 nmol/L) was transfected on day 1, then 24 hours later the promoter construct (0.3 μg) and the siRNA (50 nmol/L) were transfected (day 2). Cells then were stimulated and harvested for the indicated times. Data are reported as fold-induction over cells transfected with a control empty vector.

Measurement of PGE_2

Production of PGE_2 in the tissue culture supernatant was determined using a monoclonal enzyme immunoassay (EIA) kit (Cayman) according to the manufacturer's instructions and Morteau et al.[22] Briefly, colonic samples from TLR4−/− and WT mice were washed in cold PBS containing penicillin, streptomycin, and fungizone (100 U/mL each). A total of 100 mg of tissue fragments from each part of the colon were cultured for 24 hours in 12-well flat-bottom plates in serum-free RPMI 1640 supplemented with penicillin, streptomycin, and fungizone (100 U/mL each). Culture supernatants were harvested for PGE_2 measurement.

Flow Cytometry

Intracellular phospho-specific flow cytometry was used to quantify the effect of LPS on EGFR phosphorylation as previously described.[31,32] Briefly, LPS-stimulated or LPS-unstimulated SW480 cells were fixed in 2% paraformaldehyde at room temperature for 10 minutes. After washing with wash buffer (0.5% bovine serum albumin and 2 mmol/L EDTA in PBS), cells were permeabilized in 0.1% Triton X-100 for 5 minutes. Then cells were stained with phospho EGFR (1:500) for 30 minutes at room temperature. After 3 washes with the wash buffer, cells were incubated with TRITC-conjugated sheep anti-mouse IgG (Zymed Laboratories Inc.) for 20 minutes on ice. After washing with wash buffer, cells were filtered and analyzed by FACScan (Becton Dickinson, Franklin Lakes, NJ). Fluorescence intensity was normalized using isotype control antibody.

Cell Proliferation Assay

SW480 cells (5×10^4 cells/well) were cultured in 96-well plates in the absence or presence of AG1478 (10 μmol/L) in low serum condition (1% fetal calf serum), and stimulated with LPS (2 μg/mL). After 12 or 24 hours of stimulation, cell proliferation was analyzed using CellTiter 96 aqueous nonradioactive cell proliferation assay kit (Promega, Madison, WI). Cell proliferation was detected by measurement of formazan product in each well at the absorbance of 490 nm after incubation with tetrazolium/phenazine methosulfate for 1 hour at 37°C. The cell proliferation index was calculated as a percentage of the absorbance in relation to the untreated control cells.

Statistical Analysis

Calculation of the Student *t* test and standard deviation (SD) were performed using the statistics package within Microsoft Excel (Microsoft, Redmond, WA). Standard error was

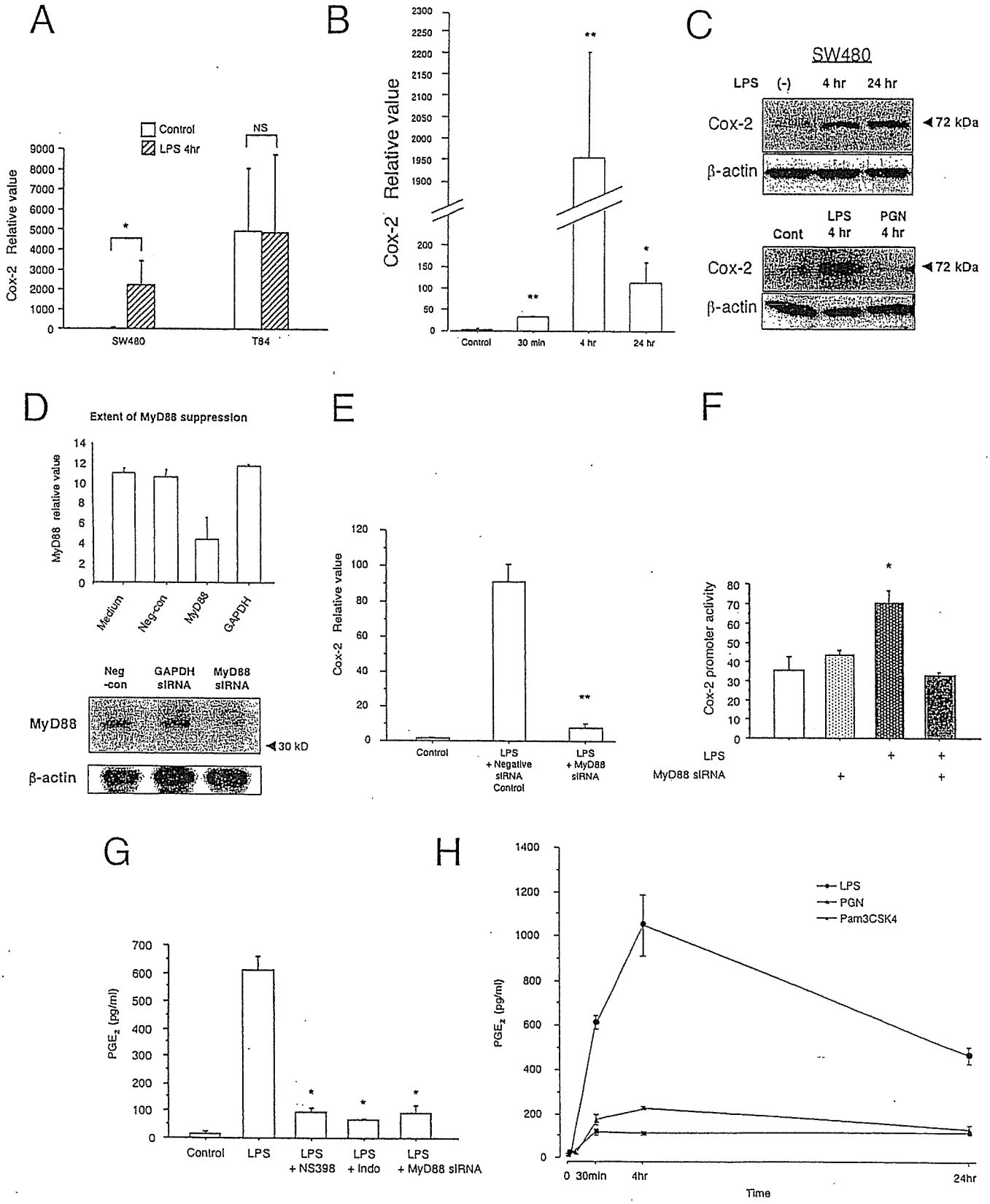
A
Control
LPS 4hr
NS
Cox-2 Relative value
SW480
T84
B
Cox-2 Relative value
Control
30 min
4 hr
24 hr
C
SW480
LPS (-) 4 hr 24 hr
Cox-2
β-actin
72 kDa
Cont LPS 4 hr PGN 4 hr
D
Extent of MyD88 suppression
MyD88 relative value
Medium
Neg-con
MyD88
GAPDH
Neg -con
GAPDH siRNA
MyD88 siRNA
MyD88
β-actin
30 kD
E
Cox-2 Relative value
Control
LPS + Negative siRNA Control
LPS + MyD88 siRNA
F
Cox-2 promoter activity
LPS
MyD88 siRNA
G
PGE2 (pg/ml)
Control
LPS
LPS + NS398
LPS + Indo
LPS + MyD88 siRNA
H
PGE2 (pg/ml)
LPS
PGN
Pam3CSK4
0 30min 4hr 24hr
Time

calculated with Stat View (Abacus Concept, Berkeley, CA). *P* values less than .05 were considered significant.

Results

Cox-2 Expression and PGE_2 Production by Intestinal Epithelial Cells Is TLR4 and MyD88 Dependent

Previous studies have shown that TLR4 signaling is involved in regulating Cox-2 expression in RAW264.7 cells.[33] We hypothesized that TLR4 also was important for Cox-2 expression by intestinal epithelial cells. To address this question, we compared the effect of LPS on Cox-2 expression in a cell line that expresses TLR4 and activates nuclear factor κB in response to LPS (SW480) vs a cell line that does not express TLR4 and is LPS unresponsive (T84).[13,34] The baseline expression of Cox-2 differed in these neoplastic cell lines.[35] Only TLR4-responsive SW480 cells increased expression of Cox-2 in response to LPS (Figure 1*A*). Induction of Cox-2 proceeded with rapid kinetics occurring within 30 minutes of LPS stimulation and peaking at 4 hours (Figure 1*B*); protein expression for Cox-2 remained increased at 24 hours after LPS stimulation (Figure 1*C*). No induction of Cox-2 protein was seen after stimulation with PGN, a TLR2 ligand (Figure 1*C*, lower panel).

To clarify further whether LPS induction of Cox-2 requires MyD88, we transfected SW480 cells with siRNA against MyD88 or a control siRNA (Figure 1*D*). Only the siRNA specific for MyD88 inhibited LPS-mediated expression of Cox-2 RNA. Finally, we asked whether LPS could induce Cox-2 promoter activation and whether this also depended on MyD88. A full-length Cox-2 promoter-luciferase construct was transfected into cells in the presence or absence of siRNA against MyD88 (Figure 1*E*). LPS activated the Cox-2 promoter and this activation was blocked by MyD88 siRNA. We performed dose-ranging studies using the Cox-2 promoter-reporter gene and found no difference in induction of the reporter between 2 and 5 μg/mL of LPS (data not shown). Taken together, these data show that LPS can directly induce Cox-2 promoter activity, messenger RNA (mRNA) expression, and protein expression in a TLR4- and MyD88-dependent fashion in colonic epithelial cells.

Cox-2 metabolizes arachidonic acid released from the plasma membrane to generate prostanoids such as PGE_2. PGE_2 in turn mediates many of the biologic effects of Cox-2 in the intestinal epithelium.[36] LPS previously has been shown to stimulate PGE_2 production by intestinal epithelial cell lines,[37-39] although most studies have attributed the biologic effects of LPS in the gut to macrophages and other stromal cells.[40] We hypothesized that LPS-mediated induction of PGE_2 depended on MyD88 signaling. Our results show that LPS induces PGE_2 production by SW480 cells (Figure 1*F*). PGE_2 production could be blocked by expression of MyD88 siRNA to an extent that was similar to a selective Cox-2 inhibitor or a nonselective Cox inhibitor, indomethacin. By contrast, stimulation with the TLR2 ligands PGN and PamCysk3 induced very little less PGE_2, especially when compared with LPS (Figure 1*G*). These data suggest that LPS stimulation of TLR4 leads to Cox-2 expression and the production of PGE_2 by intestinal epithelial cells in vitro.

Figure 1. LPS induces Cox-2 expression in human intestinal epithelial cell lines in a TLR4- and MyD88-dependent fashion. (*A*) Cox-2 expression after stimulation with LPS (2 μg/mL) in T84 (LPS unresponsive) and SW480 (LPS responsive) human intestinal epithelial cell lines. TaqMan real-time PCR showed inducible Cox-2 expression stimulated by LPS in SW480 cells. LPS-unresponsive T84 cells showed no change in Cox-2 expression in response to LPS stimulation. Data are represented as mean ± SEM of relative values of expression in 3 individual experiments of triplicate samples (*$P < .05$). (*B*) LPS-responsive SW480 cells were stimulated with LPS (2 μg/mL) for indicated times. TaqMan real-time PCR shows LPS-induced expression of Cox-2 mRNA with a peak at 4 hours of stimulation. Data are represented as mean ± SEM of relative values of expression in 3 individual experiments of triplicate samples (*$P < .05$, **$P < .001$). (*C*) Western blot analysis of Cox-2 protein expression in SW480. Cells were stimulated with LPS for indicated periods in *top panel*. *Lower panel* shows stimulation of cells with LPS (2 μg/mL) or PGN (2 μg/mL). Blots of whole-cell lysates (25 μg/*lane*) were probed with Cox-2 antibody. Data are 1 of 3 representative experiments with similar results. β-actin was used as an internal control for protein loading. (*D*) Extent of MyD88 suppression by siRNA. SW480 cells were transfected transiently with siRNA against MyD88 or glycerol dehyde-3-phosphate dehydrogenase (GAPDH). Negative siRNA, which has no significant homology to any gene sequences, was applied as a control. The knock-down efficiency of siRNA against MyD88 was assessed by real-time PCR and Western blot. The siRNA decreased both MyD88 mRNA and protein expression. Negative siRNA and siRNA against GAPDH did not affect MyD88 mRNA or protein expression. (*E*) MyD88-dependent induction of Cox-2 in response to LPS. SW480 cells were stimulated with LPS (5 μg/mL) for 4 hours and cotransfected with either MyD88 siRNA or negative control siRNA. Untransfected control samples were not LPS treated. TaqMan real-time PCR showed LPS-induced expression of Cox-2 in negative control siRNA samples. This induction of Cox-2 by LPS was largely abolished in the cells in which MyD88 was blocked with siRNA, indicating a MyD88-dependent pathway. Data are represented as mean ± SEM of relative values of expression in 3 individual experiments of triplicate samples (**$P < .001$). (*F*) LPS regulation of Cox-2 gene promoter activity. The intestinal epithelial cell line SW480 was cotransfected with the Cox-2 (−1432/+59) luciferase reporter construct, MyD88 siRNA, or the empty pGL3 vector control, together with an internal control pRL-KT (Renilla luciferase) plasmid. Cells were stimulated with LPS (5 μg/mL) for 4 hours. Reporter gene activation was significantly higher in cells stimulated with LPS than nonstimulated cells. MyD88 siRNA abrogated promoter activation in response to LPS. Data are represented as mean ± SEM of relative light units in 3 individual experiments with triplicate samples (*$P < .05$). (*G*) LPS-induced PGE_2 production in the intestinal epithelial cell line SW480. Cells were stimulated with LPS (2 μg/mL) for 30 minutes. PGE_2 concentration in supernatant was measured by monoclonal EIA. LPS stimulation resulted in PGE_2 production within 30 minutes. MyD88 siRNA inhibited LPS-induced PGE_2 production, as did a selective Cox-2 inhibitor (NS398 5 μmol/L) or a Cox-1/Cox-2 inhibitor (indomethacin 5 μmol/L). Data are represented as mean ± SEM of 2 individual measurements of duplicate samples taken from 3 individual experiments (*$P < .05$). (*H*) Effect of TLR2 ligands on production of PGE_2 compared with the TLR4 ligand LPS in the intestinal epithelial cell line SW480. SW480 was stimulated with a TLR4 ligand LPS (2 μg/mL), or TLR2 ligands PGN (2 μg/mL) or Pam3CSK4 (500 ng/mL) for indicated periods of time. The concentration of PGE_2 was examined by monoclonal EIA. There were significant differences in the stimulation of PGE_2 between LPS vs TLR2 ligands. Data are represented as the mean ± SD of triplicate samples taken from 2 individual experiments ($P < .05$, between LPS and PGN or Pam3CSK4 for each time period).

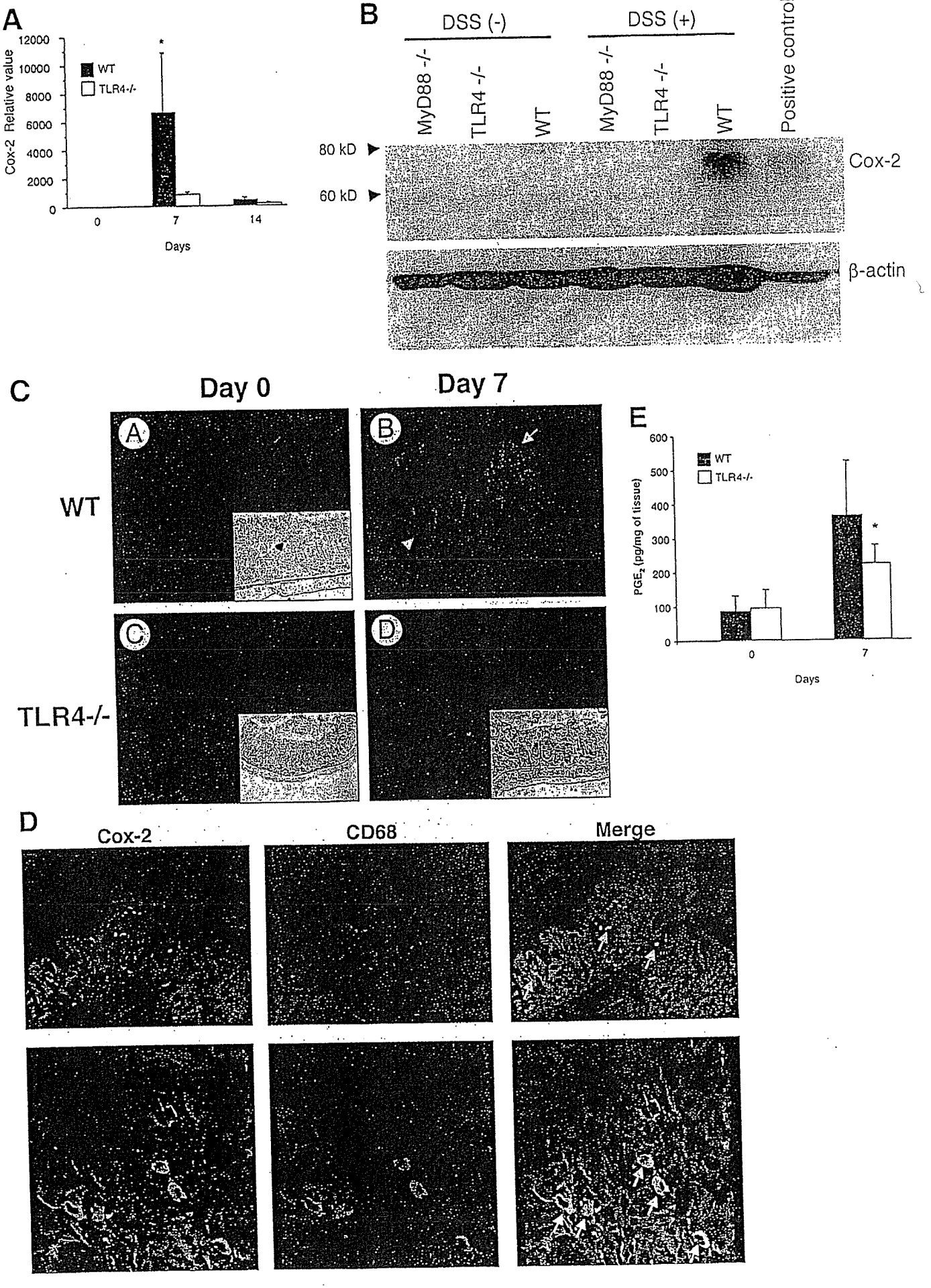
A
Cox-2 Relative value
12000
10000
8000
6000
4000
2000
0
WT
TLR4-/-
*
0
7
14
Days
B
DSS (-)
DSS (+)
MyD88 -/-
TLR4 -/-
WT
MyD88 -/-
TLR4 -/-
WT
Positive control
80 kD
60 kD
Cox-2
β-actin
C
Day 0
Day 7
WT
TLR4-/-
A
B
C
D
E
PGE2 (pg/mg of tissue)
600
500
400
300
200
100
0
WT
TLR4-/-
*
0
7
Days
D
Cox-2
CD68
Merge

Cox-2 and PGE_2 Expression Are Decreased in TLR4-Deficient Mice After DSS-Induced Injury

Cox-2 expression is increased in human IBD and animal models of colitis including DSS.[22,41] Based on our in vitro findings, we hypothesized that TLR4 signaling was important for Cox-2 expression in the setting of DSS colitis. By using real-time PCR we found that Cox-2 expression is low in WT and TLR4−/− mice before DSS treatment (Figure 2*A*), whereas Cox-1 is expressed abundantly in both (data not shown). After induction of colitis, there is a dramatic increase in expression of Cox-2 in WT mice. This up-regulation is not seen in TLR4−/− mice. We confirmed protein expression of Cox-2 by Western blot analysis of tissue lysates (Figure 2*B*) and immunofluorescence (Figure 2*C*). Colonic tissue from WT mice or LPS-treated RAW cells expressed Cox-2, but little was present in TLR4−/− colon tissue. Immunofluorescent studies revealed both epithelial staining and lamina propria staining of Cox-2 in WT mice. To define the cell types expressing Cox-2 in the lamina propria of WT mice, we performed double staining with a macrophage marker CD68 and anti-Cox-2 antibody (Figure 2*D*). Most Cox-2–positive cells in the lamina propria were also CD68 positive, suggesting that lamina propria macrophages express Cox-2 in the inflamed colon. These data support a role for TLR4 regulation of Cox-2 expression in the intestine.

Given that mice that are deficient in TLR4 do not express Cox-2, we hypothesized that TLR4−/− mice would have decreased production of PGE_2. To test this hypothesis, we measured production of PGE_2 from colonic tissue using monoclonal EIA. Our data show that PGE_2 production by colonic tissues is reduced significantly in TLR4-deficient mice after DSS-induced injury (Figure 2*E*). PGE_2 production in TLR4−/− mice was decreased by 40% compared with WT mice after DSS colitis. These data suggest that at least one defect in TLR4−/− mice with respect to epithelial repair is reduced production of local PGE_2.

TLR4−/− Mice Have Decreased Proliferation and Increased Intestinal Epithelial Cell Apoptosis After DSS-Induced Colitis

Cox-2 knock-out mice show increased susceptibility to DSS colitis similar to what we have observed in TLR4−/− mice. We have previously described that TLR4−/− mice have decreased intestinal epithelial proliferation after acute DSS-induced injury.[15] Given our findings of decreased Cox-2 expression, we wished to examine the effect of TLR4 deficiency on baseline levels of proliferation, at the peak of injury, and 7 days after recovery (day 14). By using BrdU labeling of proliferating intestinal epithelial cells, we show that proliferation is similar in WT and TLR4−/− mice before DSS treatment (Figure 3*A* and 3*B*). After DSS-induced injury, WT mice have a large increase in proliferating cells that persists even a week after DSS is discontinued. By contrast, TLR4−/− mice have significantly fewer proliferating cells. By using computerized microscopic measurements, we found a significant decrease in crypt height in the injured TLR4−/− gut that can be appreciated in the photomicrographs (Figure 3*A*) (day 7: WT, 291 ± 48.2 μm; TLR4−/−, 214 ± 20.2 μm; $P < .0001$; day 14: WT, 257 ± 111 μm; TLR4−/−, 167 ± 35.1 μm; $P < .0001$). Importantly, crypt height is similar at baseline in WT and TLR4−/− mice, suggesting this defect in proliferation is only apparent in the setting of injury (day 0: WT, 244 ± 72.9 μm; TLR4−/−, 251 ± 49.5 μm; $P < .321$).

Colonic crypt height represents the balance of epithelial proliferation and apoptotic cell loss at the top of the crypts.[28,42] We reasoned, therefore, that TLR4−/− mice could have increased intestinal epithelial cell apoptosis in response to DSS injury. To address this question, we performed TUNEL staining on intestinal sections from DSS-treated TLR4−/− mice or their WT controls (Figure 3*C* and *D*). We found significantly more apoptotic cells per crypt in TLR4−/− intestine compared with controls. In general, the apoptotic cells were found at the tops of the colonic crypts. Similar findings were seen in MyD88−/− mice, suggesting this was an MyD88-dependent phenomenon (data not shown). An increased rate of apoptosis was not seen in the intestines of mice before DSS treatment. We conclude from these data that TLR4 is important for intestinal epithelial repair from injury by aiding in proliferation and protecting against apoptosis.

PGE_2 Restores Proliferation and Protects Against Apoptosis in TLR4−/− Mice

We have shown previously that TLR4 is required for induction of Cox-2 and PGE_2 during DSS-induced injury. We hypothesized that the decrease in PGE_2 production in TLR4−/− mice was responsible for the observed phenotype,

Figure 2. Cox-2 expression is decreased in TLR4−/− mice after DSS-induced colitis. (*A*) TaqMan real-time PCR showed up-regulation of Cox-2 expression in the colon of WT mice but not in TLR4−/− mice after 7 days of DSS treatment (n = 3 for each group on day 0, n = 12 for the other groups). Data are represented as the mean ± SEM of relative values of expression in 4 individual experiments (*$P < .05$). (*B*) Western blot analysis for Cox-2 in the colon. Immunoblots of tissue lysate proteins (25 μg/lane) prepared from colonic samples of TLR4−/− and MyD88−/−, and WT control mice before and after 7 days of DSS treatment. Membranes were probed with Cox-2 antibody. Positive control consists of cell lysate from LPS (2 μg/mL)-stimulated RAW264.7 cells (*right lane*). Cox-2 protein expression was greater in WT colon. Data are 1 representative experiment of 3 independent studies. β-actin was used as an internal control for protein loading. (*C*) Immunofluorescent staining for Cox-2 in the colon before and after 7 days of DSS treatment. Before DSS treatment, colonic tissue does not express detectable levels of Cox-2 in either (*C*) TLR4−/− mice or (*A*) WT controls. Immunofluorescent signal (*red* color of rhodamine) of Cox-2 was strongly detected in the colonic epithelial cytoplasm (*arrow*) and lamina propria cells (*arrowhead*) in (*B*) WT mice, but is very low in (*D*) TLR4−/− mice after DSS treatment. *Insets* show phase-contrast images identifying the orientation of colonic sections. (*D*) Expression of Cox-2 by lamina propria macrophages using double-staining of Cox-2 (fluorescein isothiocyanate green) and CD68 (TRITC *red*). Most Cox-2–positive lamina propria cells were double-stained with CD68 (macrophage marker). Representative data are from WT mice treated with 7 days of DSS. *Arrows* indicate double-positive cells showing *yellow* cytoplasmic staining. TLR4−/− mice do not have Cox-2–positive lamina propria macrophages (see *C*). (*E*) PGE_2 production in DSS-induced colitis. Colonic tissues from TLR4−/− and WT controls before and after 7 days of DSS were cultured in media for 24 hours and the concentration of PGE_2 in the supernatants was analyzed by EIA (n = 4 for each group). Data are represented as the mean ± SD of duplicate samples taken from 3 individual experiments. There was a significant difference in PGE_2 production in TLR4−/− mice after DSS treatment compared with WT mice (*$P < .05$).